CATÓLICA
ESCOLA SUPERIOR DE BIOTECNOLOGIA
PORTO

OPTIMIZATION OF CHITOSAN-HYDROXYAPATITE-BASED BIOINKS FOR POTENTIAL 3D BIOPRINTING APPLICATION IN BONE TISSUE REGENERATION

by
Ana Helena Alves da Costa

November 2022

CATÓLICA
ESCOLA SUPERIOR DE BIOTECNOLOGIA
PORTO

OPTIMIZATION OF CHITOSAN-HYDROXYAPATITE-BASED BIOINKS FOR POTENTIAL 3D BIOPRINTING APPLICATION IN BONE TISSUE REGENERATION

Training Placement Report presented to *Escola Superior de Biotecnologia of the Universidade Católica Portuguesa* to fulfill the requirements of Master of Science degree in Biomedical Engineering

by
Ana Helena Alves da Costa

Supervision: Clara Piccirillo – Supervisor
Francesca Scalera – Co-Supervisor
Tutor (Escola Superior de Biotecnologia): Prof. Ana Leite Oliveira

November 2022

RESUMO

Com o passar dos anos, a evolução científica contribuiu muitas vezes para a medicina, fornecendo soluções, para o que pareciam ser, problemas para toda a vida. Nem todos os problemas de saúde podem ser resolvidos com tratamentos tradicionais, pois nem todas as complicações são causadas por doenças tratadas com medicamentos. Isto é especialmente verdade com problemas relacionados com os ossos. Idade, acidentes ou defeitos congênitos podem ser culpados por deformidades esqueléticas graves que não podem ser tratadas por conta própria. Esta necessidade de criar novas soluções para auxiliar na medicina, despertou o interesse da comunidade científica. Atualmente, podemos contar com um grande número de opções para ajudar no reparo e regeneração óssea, particularmente *scaffolds 3D* bioimpressos.

Neste estudo, o principal objetivo foi criar e otimizar um biomaterial que pudesse ser usado como *bioink* para criar estruturas bioimpressas em 3D para futura aplicação em regeneração óssea. O material utilizado consistiu num hidrogel à base de quitosano com incorporação de hidroxiapatita (HA), que é conhecido como o fosfato de cálcio mais comum presente no osso humano. A HA sintética (SYN_HA) foi sintetizada e mostrou ser um material adequado para a preparação de um hidrogel; HA natural (NAT_HA) de espinhas de atum, no entanto, também se mostrou uma alternativa muito interessante, embora ainda exija algum trabalho adicional. No futuro, com condições de preparo otimizadas, seria uma opção mais sustentável para os pacientes.

Vários testes foram realizados no hidrogel, para otimizar a sua composição, em particular a concentração de HA mais adequada para incluir no próprio hidrogel. Foram realizados testes nos nanocristais para avaliar sua pureza e cristalinidade, bem como o tamanho das partículas. Estes foram seguidos por testes para comparar hidrogéis com duas percentagens finais de HA: 0.125% p/vol e 0.25% p/vol. As seguintes análises foram realizadas: um teste de estabilidade para estudar a cinética de degradação do hidrogel *in vitro* em condições fisiológicas; análise de pH, homogeneidade e polimerização; um teste de compressão para avaliar as propriedades mecânicas do hidrogel, particularmente a rigidez; um teste de bioimpressão, pelo método de extrusão manual, que avaliou a sua capacidade de formar fibras sem se misturar, para formar construções 3D. Todas estas eram pré-condições para determinar se os hidrogéis se comportariam bem como uma *biomaterial ink* e para uso futuro em testes de viabilidade celular.

O teste final foi a bioimpressão do material onde os parâmetros foram otimizados, para garantir sempre uma reprodução bem-sucedida das estruturas impressas.

Os resultados mostraram que o biomaterial com melhor concentração de SYN_HA foi o de 0.125% p/vol, pois apresentou os resultados mais satisfatórios em todos os testes realizados, confirmando que pode ser utilizado para fins de bioimpressão.

Palavras chave: bioink; bioimpressão; regeneração óssea; hidrogel de quitosano; hidroxiapatite.

ABSTRACT

With the passing of the years, scientific evolution has contributed many times to medicine by providing solutions to, what seemed to be, life-long problems for patients. Not all health problems can be fixed with traditional treatments, as not all complications are caused by drug treated diseases. This is especially true with bone related issues. Age, accidents or birth defects can all be at fault for serious skeletal defects that cannot be treated on their own. This necessity to create further solutions to aid in medicine, arose an interest in the scientific community. Fast forward to this day and age, we can now count on a vast number of options to help in bone repair and regeneration, particularly 3D bioprinted scaffolds.

In this study, the main goal was to create and optimize a biomaterial that could be used as an ink to create 3D bioprinted structures for future bone regeneration application. The material used consisted of a chitosan (Ch) -based hydrogel with the incorporation of hydroxyapatite (HA), which is known as the most common calcium phosphate present in human bone. Synthetic HA (SYN_HA) was synthesized and showed to be a suitable material for hydrogel preparation; natural HA (NAT_HA) from tuna fish bones, however, also looked as a very interesting alternative, although it still requires some additional work. In the future, with optimized preparation conditions, it would be more sustainable option for patients.

Several tests were performed on the hydrogel, to optimize its composition, in particular the most appropriate concentration of HA to include in the hydrogel itself. Tests on the nanocrystals to assess their purity and crystallinity as well the particle size were performed. These were followed by experiments to compare hydrogels with two final HA percentages: 0.125% wt/vol and 0.25% wt/vol. The following analysis were performed: a stability test to study *in vitro* hydrogel degradation kinetics under physiological conditions; pH, homogeneity and polymerization assessments; a compression test to evaluate mechanical properties of the hydrogel, particularly the stiffness; a bioprintability test, by a hand-extrusion method, that assessed its capability to form fibers without merging, to form 3D constructs. All of these were pre-conditions to determine if they would behave well as a biomaterial ink and for future use on cell viability trials.

The ultimate test was the bioprinting of the material where the parameters were optimized, to guarantee a successful reproduction of the printed structures every time.

Results showed that the biomaterial with the best concentration of SYN_HA was the 0.125% wt/vol one, as it had the most satisfactory results in all tests performed, confirming it can be used for bioprinting purposes.

Keywords: bioink; bioprinting; bone regeneration; chitosan-based hydrogel; hydroxyapatite.

AKNOWLEDGEMENTS

First and foremost, I would like to thank Professor Clara Piccirillo for her patience and guidance during this project as well as during my stay in Italy. She, along with many others in NANOTEC, welcomed me with open arms and helped me during times of distress. I would like to also thank Francesca Scalera for being tremendously helpful and concerning during my pratical and writing times. I will never forget your help.

Besides, i would like to thank Universidade Católica Portuguesa for providing me with an amazing opportunity to fulfill my wish of studying/working abroad.

Any attempt at any level can't be satisfactorily completed without the support and guidance of my family and friends.

As such, i would like to say how grateful i am for my parents and sister who have supported me always, but specially during this last year, as life abroad could be a little overwhelming at times. No amount of *thank you* will ever be enough.

Last but not least, I would like to thank my friends. Friends that became like family, friends i made during my stay in Italy which i will never forget and friends from home who i will carry with me forever.

CONTENTS

1. INTRODUCTION

1.1 3D bioprinting for bone regeneration

A bone birth defect, trauma caused by an accident or skeletal complications associated with old age or cancer may all cause restrains in mobility. Although less vulnerable patients can overcome these complications, in some cases pain aid, or physical therapy is not enough.

As the treatment of bone abnormalities remains a partly unresolved clinical challenge, bone tissue engineering is a growing topic of study. The most common technique is to take mesenchymal progenitor cells or osteoblasts from the patient and develop enough tissue *in vitro* on implantable, three-dimensional scaffolds to utilize as a bone replacement. Tissue engineering aims to create effective cell-material structures in vitro by combining "intelligent," bioresorbable scaffold materials with appropriate growth factors to enhance cell adhesion, proliferation, and differentiation.[1]

The ability of bone tissue to tolerate and adapt to mechanical stressors, as well as mend fractures, is due to a synergy between its components: bone cells, the extracellular matrix (ECM), and bioactive chemicals. Furthermore, it is recognized that a complicated cross-talk between bone building and inflammatory cells guides effective regeneration. As a result, mending a tissue whose cells are as precisely coordinated as bone is a difficult undertaking. Only autografts have all three desirable properties of an optimal bone graft: osteoconductivity, donor-site osteogenic cells, and osteoinductive factors. Because of these considerations, autografts are still regarded the gold standard for mending bone lesions, despite considerable limitations such as donor site availability and potential morbidity.[2]–[4]

To avoid the drawbacks of the present treatments stated above, researchers have focused their efforts on bone tissue engineering (BTE). This ground-breaking research field has recently been strengthened by the introduction of a set of procedures known as bioprinting, which allow for the healing of bone deformities using 3D-printed live tissues. The achievement of biomimicry and thus the possibility of avoiding an abnormal immune reaction towards grafts, the well-known foreign body reaction, which can lead to chronic inflammation, fibrosis, or scarring, and transplantation failure, is an even more compelling argument in favor of 3D-bioprinted constructs. Indeed, the various scaffolds utilized for bone implants can display distinct immune responses based on their varied physical, chemical, and biological features. In contrast, immune cells regulate osteoclastogenesis, osteogenesis, and the process of bone repair by the release of regulatory factors.[5]

In recent years, bioprinting technology has greatly increased the availability of viable synthetic-bone alternatives with better performance.

1.2 Tissue engineering 3D structures

In recent years the concept of engineering or regenerating tissues as a form of treatment became much more advanced and with concrete applications. Innovative solutions to treat defective problems such as tissue engineering and regenerative medicine were explored due to the limitations of traditional medicine.

Tissue engineering applications frequently include the use of three-dimensional (3D) scaffolds to provide an appropriate microenvironment for the integration of cells and/or growth factors in order to restore damaged tissues or organs. When compared to typical 2D monolayer culture techniques, these scaffolds mirror the actual *in vivo* milieu more closely. The added dimensionality of 3D cultures is the critical element causing changes in cellular responses. It not only influences the spatial structure of cell surface receptors involved in interactions with neighboring cells, but it also imposes physical limits on them.[6], [7]

These cell-based scaffolds are either cultivated for *in vitro* tissue synthesis before being implanted directly into the injured region, or they are put directly into the site of *in vivo* injury, where the body's own system stimulates tissue or organ regeneration. The "triple or trio of tissue engineering" (**Figure 1.1**) refers to the combination of[8]:

1. A scaffold that offers structure and substrate for tissue growth and development.
2. A supply of cells to aid in the production of needed tissues.
3. Growth factors or biophysical cues to direct cell proliferation and differentiation inside the scaffold.[9]

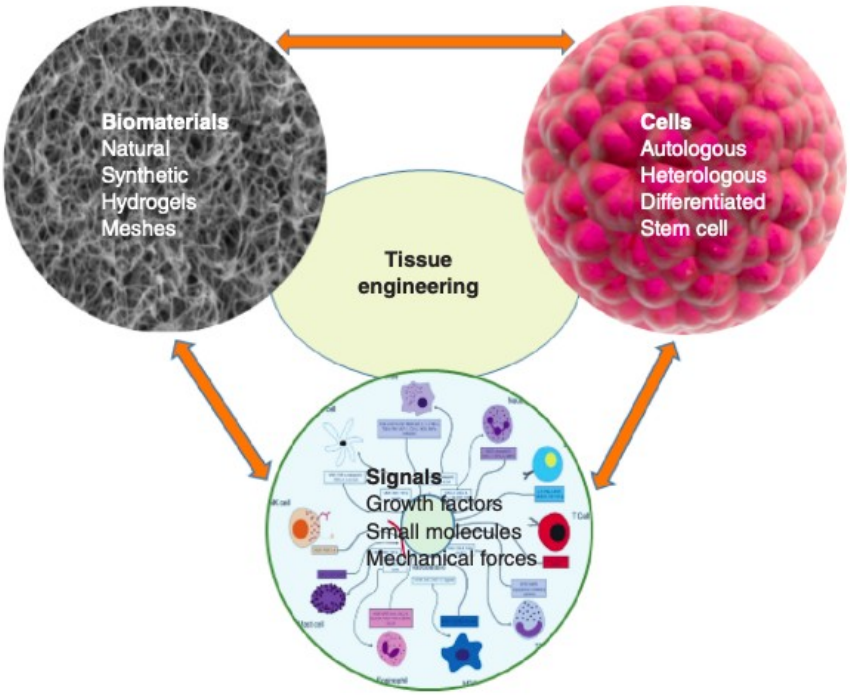

Figure 1.1 *The triad of tissue engineering. The combination of cells, scaffolds, and signals is used to engineer functional tissues.*[10]

A scaffold's design must meet mechanical, physicochemical, and biological criteria. Shape, size, strength, porosity, and degradation rate of 3D scaffolds should all be easily modified to optimize bioactivity and efficiency. To heal the injured tissue, the scaffold should be developed and manufactured in a manner that mimics the function and biomechanics of the original tissue. To achieve this objective, the 3D scaffold should be able to temporarily endure the external pressures and stresses induced by new tissue growth, while retaining mechanical qualities similar to the surrounding tissue.[11] At the same time, the rate of degradation should match that one of tissue growth, without the formation and release of harmful byproducts. This characteristic will also help when it comes to biocompatibility as no toxic, immunological, or foreign body reactions should arise when the implant is properly placed in the body. The scaffold's surface qualities should also be engineered to allow cell adhesion, uniform dispersion, proliferation, and cell-to-cell interactions. For example, its shape should be porous or fibrous, with a high surface-to-volume ratio for cell adhesion and tissue growth. Finally, size wise, nanostructured surfaces have a high surface energy, which leads to strong protein adhesion and cell attachment.[12]

Cells can be mainly divided into three categories: autologous, allogenic, or xenogenic. Autologous cells are obtained directly from the individual receiving repair, whereas allogenic cells are harvested from a donor (of the same species). Xenogenic cells are transplanted from

another species, and they are less prevalent in tissue engineering than in full organ transplantation.

For treating damaged or wounded tissues in patients, there are three main cell therapy strategies:

1. Implanting isolated cells: Using this method, complete cell populations can be transplanted directly, or isolated cells can be grown and expanded *ex vivo* prior to re-implantation.

2. Implanting a construct assembled from cells and scaffolds: provide a mixture of whole cell isolates or ex vivo grown cells planted onto a substrate template. Apart from implantation outcomes, implant designs are still often evaluated in vitro employing 3D culture systems.

3. *In situ* tissue regeneration by native cells: The recruitment of native cells to areas of tissue injury. In other words, it is the migration and tissue-specific differentiation of endogenous progenitors, which is influenced by drugs that modify regulatory signals, proteins, or the use of gene therapy technology.[9]

Following an injury, a series of biological activities such as stem cell migration, chemokine and growth factor production take place to heal the damaged tissue. In this approach, the designed complex scaffolds should imitate the natural signaling and the healing processes and create an appropriate environment for stem cell adhesion, proliferation, and differentiation to regenerate the tissue. In particular, *in vivo* bone production necessitates the release of chemicals at important time periods to drive osteoinduction; indeed bone regeneration can be significantly accelerated by targeted supply of suitable growth factors. [13]

Considering all the issues to fabricate a 3D scaffold possessing all necessary requirements, many techniques were developed to obtain a simpler, more reproducible and standardized 3D cell model (fiber bonding, phase separation, solvent casting, etc.). However, all of these approaches show one main limitation, as they do not provide for enough control over scaffold design, pore network, and pore size; this results in inconsistent and less-than-ideal 3D scaffolds. To address this issue, researchers proposed using 3D printing technology to create tailored scaffolds with regulated pore size and structure.[14]

1.3 3D bioprinting technology

3D printing is a mechanical method that produces solid items by 'printing' successive layers of material to reproduce a computer-modeled design.[15] [16]

Although the notion of 3D printing is gaining popularity, the principles, software, and even instruments used to create it have a much older history. Concepts and technology connected to 3D printing may be traced back at least 40 years, according to US Patent Office documents. While Selective Laser Sintering (SLS), in which a laser is used to sinter powdered material, generally a metal, by heat, was one of the first methods used for 3D printing, various other patented procedures are now prevalent. These numerous processes can have an impact on future advances in various fields, including biomedicine. The features of the different 3D models created by different printing technologies make them desirable to different applications. Aside from the one mentioned earlier, the three most common types of 3D printing are: stereolithography (SLA), which requires the focusing of an ultraviolet (UV) laser on a vat of photopolymer resin, solidifying it; electron beam melting (EBM), in which metal powder or wire is welded together using an electron beam as the heat source; and 3D bioprinting.[16]

Bioprinting is a 3D manufacturing process that accurately dispenses cell-laden biomaterials for the building of complex 3D functioning live tissues or artificial organs.[17] Because of its versatility and prospective applications, 3D bioprinting is becoming significant in biomedicine. In general, bioprinting applications are divided into two categories: (1) tissue regeneration, such as printing vascular grafts, heart valves, bone, liver, neurons and skin; and (2) biological applications, such as drug development and biopreservation.[18] In comparison to the traditional use of 3D printing to form cell-free scaffolds, 3D bioprinting necessitates different technical approaches, such as biomimicry, autonomous self-assembly, and mini-tissue building blocks; they are then used to construct 3D structures with mechanical and biological properties suitable for the deposition of living cells and the restoration of tissue and organ function.[19] 3D bioprinting has various benefits over traditional 3D printing, including precise cell dispersion, high-resolution cell deposition, scalability, and cost-effectiveness. However, numerous hurdles remain in the development and subsequent uses of 3D bioprinting in medicine. [20] The key problem is the difficulty to duplicate the intricate micro-architecture of extracellular matrix (ECM) components and various cell types with enough detail to mimic biological function.[19]

The creation and characterization of novel bioinks has attracted growing interest, particularly as a scarcity of materials suited for bioprinting has been cited as one of the key impediments to rapid advancement in the area.[21]

Models can be created using CAM software's resulting 2D or even 3D structures.

1.3.1 Extrusion-based bioprinting: principle, advantages and limitations

Extrusion-based bioprinting (EBB) (**Figure 1.2**) is a fast-evolving technology in biomedical engineering that has achieved significant progress in the creation of medicinal constructs. Cell-laden hydrogels or bio-inks are extruded layer by layer onto printing stages to build three-dimensional (3D) constructions of varied sizes, shapes, and resolutions.[22] EBB employs a continuous force, generated by a pneumatic pressure or piston, to extrude an unbroken line of bioink rather than liquid droplets, through a micro-nozzle. After solidifying on the substrate, the extruded material serves as a support structure; the platform is then lowered horizontally and another layer of bioink is added until the whole 3D build is completed. Mechanical dispensing printers, such as piston and screw-based printers, allow more direct control over the material flow, resulting in higher spatial control, due to a delay in the compressed gas volume in pneumatic systems.[20] The viscosity and density of the bioink, the liquid phase of the bioink, the extrusion speed, and other material-specific characteristics, such as the capacity to cross-link between printed layers, are some of the most important parameters to consider for achieving quality products via extrusion bioprinting.

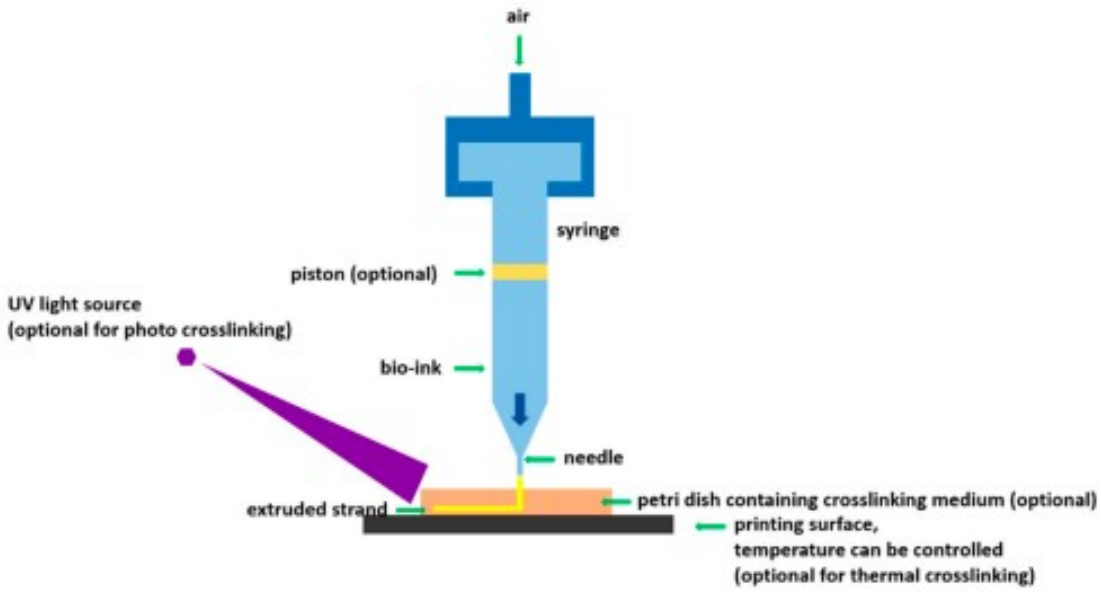

Figure 1.2 *Schematic of extrusion-based bioprinting using various crosslinking mechanisms.*[22]

One of the most significant benefits of extrusion bioprinting is the capacity to deposit a high density of cells, allowing for a more diverse range of material choices with a variety of cell densities and viscosities. Extrusion bioprinting acquires structural support with printed components when using high-viscosity materials, but low-viscosity materials can be used to provide a more ideal environment for preserving cell survival and function.[19] It offers faster deposition and printing speeds, which can help with scalability in a short amount of time. The final and most crucial argument is that EBB allows for the bioprinting of anatomically accurate porous constructions, which is extremely difficult with conventional methods.[23]

Despite its adaptability and numerous advantages, EBB has some drawbacks when compared to other technologies like droplet-based bioprinting, inject-based electrohydrodynamic and laser-based bioprinting. To begin with, the technology's resolution is quite restricted; the minimum feature size is often greater than 100 μm, which is far lower than the resolution of the other bioprinting processes. As a result of the restricted resolution, cells cannot be accurately designed and ordered. Furthermore, the bioink in liquid or sol-gel form must have shear thinning capacity to overcome surface tension-driven droplet formation, to be successfully extruded as cylindrical filaments. The hydrogels utilized in EBB are limited by the gelation and solidification needs during the extrusion process. Furthermore, when the cell density is high, shear stress on the nozzle tip wall causes a considerable decline in the number of live cells. Cell viability is also affected by the time it takes to bioprint massive structures.[23]

1.4 Hydrogels for 3D Bioprinting

Regardless of the 3D bioprinting approach, bioink is a crucial component of this technology. As described by Groll et al. [24], *'a formulation of cells suitable for processing by an automated biofabrication technology that may also contain biologically active components and biomaterials'*. The production of biological structures, particularly their mechanical and cellular behavior, is greatly influenced by bioink synthesis, bioprinting, and cross-linking. As a result, bioink is one of the most important components of 3D bioprinting, and it is inextricably linked to the bioprinting technology and the chosen cells.[25]

A very common example of a material used as biomaterial ink (possible bioink) is hydrogels. Hydrogels are vital in bioprinting. They not only come into close contact with cells to give structural support, but they also have a strong influence on the chemical and physical characteristics of bioinks.[26]

1.4.1 Definition and properties

Hydrogels are three-dimensional (3D) cross-linked polymer networks; one key property is their capacity to absorb and hold large volumes of water while remaining stable in structure. [27]

Since hydrogels will be the base for the construction of the 3D scaffolds, many of its characteristics and requirements are the same already listed above for scaffolds

The most important factor is the biocompatibility of the materials. Furthermore, the hydrogel should be immunocompatible, preventing a large inflammatory reaction in *in vivo* microenvironments. Another critical criterion is the presence of a network of linked micropores in their structure, as this promotes the flow of gases (O_2 and CO_2), nutrients, proteins, and degradation products into and out of or within the hydrogel. This is critical for encapsulated cell viability and proliferation. The breakdown of the substance is also significant because it creates more room for cell growth, migration, and blood vessel infiltration. The capacity to reproduce the dynamic nature of the extracellular matrix (ECM), on the other hand, is seen as a primary issue in hydrogel synthesis. The capacity to form a cell-laden hydrogel matrix is heavily reliant on the intensity of the crosslinking reaction, as well as the cytotoxicity of byproducts and unreacted chemicals. The monomers, initiators, and free radicals produced by the reactions can be harmful to cells, reducing the effectiveness of the 3D microenvironment *in vitro* and *in vivo*. In addition to these generic qualities, viscosity is an important parameter for hydrogels. If the viscosity is too high, strong pressure should be applied, and the high mechanical forces and shear stresses that arise may harm the cells. Low viscosity, on the other hand, may impair structural integrity and the resolution of the printed structure. Mechanical stability is another important aspect in the development of the hydrogel system. In some cases, the mechanical characteristics of the hydrogels can have a significant impact on tissue development. The mechanical characteristics of the hydrogel, especially stiffness, are well recognized to impact cell adherence, proliferation, and differentiation. [28]

All the previous characteristics should be considered when studying the chance of creating a hydrogel for a future bioink as they function as a biomimetic ECM, stimulating tissue development and regeneration.[29]

1.4.2 Classification

Hydrogels can be classified in different ways. However, because hydrogels are essentially cross-linked networks, they can be classified into two classes, depending on their cross-linking:

- **Physically cross-linked or self-assembled hydrogel**
- **Chemically cross-linked hydrogel**

In either case, the hydrogel can derive from natural or synthetic source.[30]

Because natural hydrogels are composed of non-man-made sources, they are intrinsically biocompatible and bioactive.[31] They are suitable as a medium for cell development when excellent water retention, non-toxicity, and absence of inflammatory response are required. [32] Their main drawbacks are their low mechanical strength, batch variance, and the possibility of disease transmission from animal-derived hydrogels. Although the last one can be avoided with suitable sterilization protocols.

Synthetic hydrogels, on the other hand, are made utilizing chemical polymerization procedures and are preferable when greater durability, strength, and water absorption capacity are required. However, in some cases there may be a lack of biocompatibility, which may require chemical modification; slower degradation rates than their natural equivalents may also be experienced.[33]

Crosslinking is a stabilization method that involves changing the internal structure of the cell-laden printed hydrogel in order to harden it and retain the final shape, structure, and architecture of the bioprinted structure. The crosslink process causes the hydrogel to shift from liquid to gel form. It may be done in two ways: by exposing the construct to either chemical (e.g. UV light irradiation) or physical stimuli (for instance temperature or ionic interactions). After being crosslinked, the construct may be grown in incubators under closely regulated conditions. **Figure 1.3** enumerates all the crosslinking techniques for the preparation of a hydrogel.

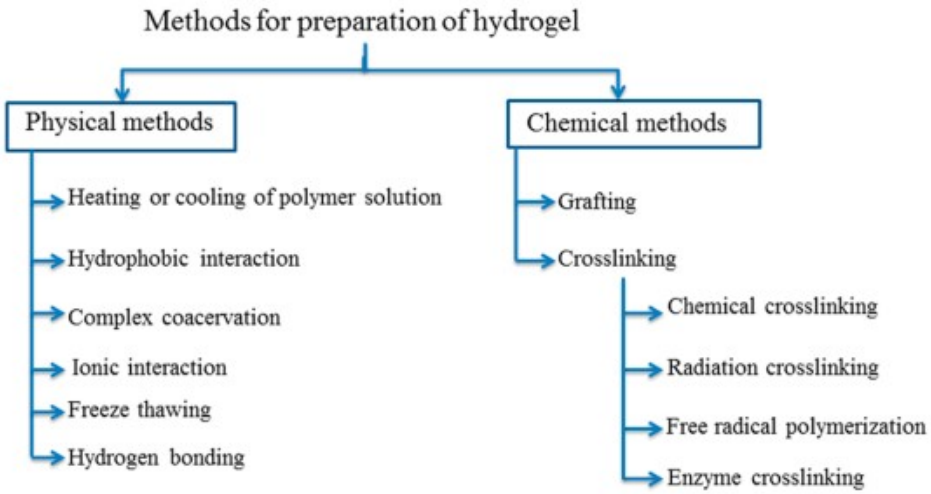

Figure 1.3 *Different methods for the preparation of hydrogels.*[34]

When compared to physically crosslinked hydrogels, chemically crosslinked hydrogels exhibit superior stability, longer durability, and higher mechanical characteristics (tensile, shear, bending, etc.). They are created by grafting functional monomers into the polymer network or by coupling the two polymer chains with a crosslinker. These chemical reactions rely on the crosslinking of polymer functional groups (-COOH, -OH, or -NH2, for example) with crosslinkers such as aldehydes (glutaraldehyde, adipic acid dihydrazide, for example) and N,N-(3 dimethylaminopropyl)-N-ethyl carbodiimide (EDC).[35]. An interesting example of chemical crosslinking is photocrosslinking. In this method, high intensity irradiation, such as UV, can be used to trigger radical processes. GelMA is an example of a photosensitive hydrogel so with the addition of a photoinitiator, molecules in hydrogel solutions are activated by UV light to induce polymerization. Crosslinking takes anywhere from a few seconds to a few minutes. [36]

Hydrophobic, electrostatic, and hydrogen bonding between polymer chains are the forces involved in physical gel formation. This indicates that gel formation may be reversed since the network creation caused by all of these interactions is entirely physical.[37] An example of a physical method in the fabrication of hydrogels is the thermosensitive hydrogel. Ideally it should be in the liquid state in the temperature range of 8-25 °C and have a transition to the gel state in the physiological temperature range of biological fluids (36-37 °C). With these features such hydrogels would be unique and ideal materials for the creation of medicinal delivery systems, soft implants *in vivo,* and 3D in vitro models. These properties are quite appealing: they enable target cell encapsulation at room temperature and, eventually, the

development of a stable hydrogel system *in situ* at body temperature without the use of additional chemical or physical stimulation.[38]

The chitosan-Betatglycerolphosphate is a good example of a hydrogel that polymerizes when placed in the physiological temperature range, but remains in a liquid state on temperatures below 25ºC. This can be particularly interesting in 3D bioprinting, as it is described in the next paragraph.

1.4.3 GelMA-LAP based hydrogel

Gelatin is a natural hydrophilic polymer derived from the hydrolysis and denaturation of bovine or porcine collagen taken from bones, skin and connective tissues under high temperature.[39]

Because of its biodegradability and biocompatibility in physiological conditions, it is frequently employed in pharmaceutical and medical applications. These properties have led to gelatin's demonstrated safety as a plasma expander, a medicine formulation component, and a sealant for vascular prosthesis. [40] Some constraints, however, including its low mechanical modulus and quick deterioration, limit its usage in biomedical applications. To overcome these drawbacks, gelatin methacrylate (GelMA) is made by chemically modifying gelatin by adding methacrylate groups to the amine-containing side groups (**Figure 1.4).**
Moreover, the methacrylate group also makes the material photoactive. In fact, in the presence of a photoinitiator, this group undergo UV-light driven polymerization of the gelatin into a hydrogel that is stable at 37ºC.

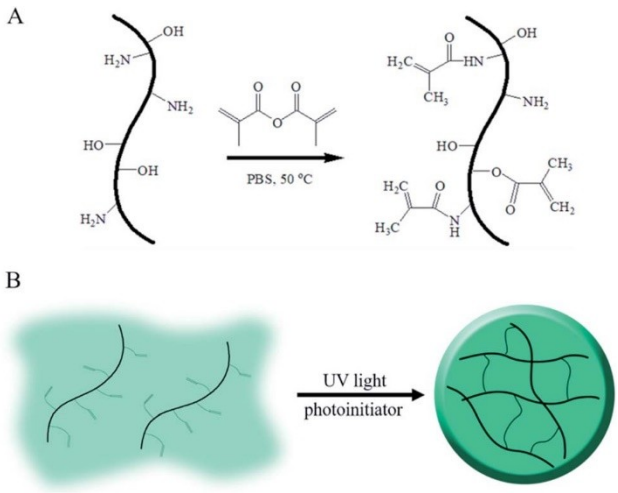

Figure 1.4 *Schematic representation of GelMA and the formation of its hydrogels through photocrosslinking.*[41]

GelMA-based biomaterials have been extensively researched for their physical and biological characteristics, with applications spanning from medication delivery to tissue engineering.[41] However, its application in 3D Bioprinting is still relatively new, thus its use as a bioink could be a major advance in the biomedical world.

1.4.4 Chitosan-BGP hydrogel

Chitosan (Ch), is a natural polymer that is derived from the exoskeleton of crustaceans. It has enormous biomedical potential as it induces a minor immune response when used for tissue engineering making it a very biocompatible material. It is also non-immunogenic and biodegradable, and its molecular structure, which is similar to glycosaminoglycans, makes it suited for ECM reproduction. [42]

When combined with a gelating agent, such as β-glycerophosphate, the interaction between the polar chains of chitosan and βGP, create the foundation of the thermoresponsive effect. This determines the hydrogel gelation between 32 and 37 °C, avoiding polymer precipitation and restores pH to normal levels.[38] Chitosan hydrogels have mostly been employed to assist cell adhesion and growth in medication delivery systems, wastewater and dye cleanup, and tissue engineering. These are employed in the biomedical and biotechnological areas for controlled release formulations of molecules such as drugs, volatile compounds, or proteins. They can be used in wound dressings to absorb the wounded area's secretion and release water on the wound surface, keeping it moist. As a result of its advantageous qualities, including as durability, permeability, flexibility, and wide application, research into its use has grown in popularity.[43]

1.4.5 Hydroxyapatite and its use in hydrogels

Hydroxyapatite ($Ca_{10}(PO_4)_6(OH)_2$ — HA) is a calcium phosphate commonly used in biomedicine. It is the most abundant (70%) and most significant component of human, animal and fish bone. Some of its properties include good osteoconductivity, osteoinductivity, and bone bonding capabilities, as well as slow disintegration *in situ*.[44] Because of these properties, HA is employed as bone substitute. The most common way to obtain HA nanocrystals is through chemical synthesis. When synthetizing it the goal is to obtain a 39.68% by weight calcium and 18% by weight phosphorus. This will mean that the resulting Ca/P mole ratio will equal to 1.67. [45] If the ratio matches the one indicated than the purity

of the nanocrystals is high. This is especially important for the application in biomedicine as high purity mean there is a lower chance of rejection of the polymers by the body.

However, it has been discovered that it can also be made from natural byproducts/waste. Because HA is the primary component of animal and fish bones, the latter's skeletons may be utilized as a raw material to produce naturally supplied HA.[46]

HA can be incorporated into hydrogels; this is likely to result in a more stable hydrogel, as HA is expected to increase stiffness, connectedness. The main advantage of HA incorporation, however, will be an enhanced osteogenic potential [47], due to HA properties described above. Such hydrogels will resemble the ECM microenvironment as close to the real one as possible.

1.5 Aim of the Thesis

The goal of this thesis was to create HA-based hydrogels for bone tissue engineering, to be used as bio-inks in 3D bio-printing processes. Two formulations were tested, employing chitosan or GelMA, termo- and photo-sensitive gels, respectively. Considering HA, both synthetic and natural HA were used. For the prepared hydrogels chemical-physical, and mechanical characterization were carried out. Finally, a printability test and printing parameter setup were performed on the created hydrogel in the RegenHU® company's 3D extrusion-based bioprinter. These tests were carried to assess whether the bioink would be suitable for cell encapsulation.

2. MATERIALS AND METHODS

2.1. Synthesis of the materials

2.1.1. Hydroxyapatite (HA)

Hydroxyapatite ($Ca_{10}(PO_4)_6(OH)_2$, HA) is a calcium phosphate ceramic, the main component of the natural bone (~70%), which is why its application in the biomedical field is so common. Its use in bone regeneration has shown that, together with another tricalcium phosphate ($CA_3(PO_4)_2$, TCP), it is the most effective bioactive ceramic to induce bone formation on its surface. Thus, it became the main component of this research. [48], [49]

Two types of HA were prepared, characterized and compared:

- **Natural HA**: derived from fish scales, tuna in this case
- **Synthetic HA**: made from a chemical reaction in the laboratory

In order for the correct particle size to be achieved, after the synthesis, some extra steps were conducted so that the resulting particles were more uniform in size and smaller, to be easily added to a hydrogel.

2.1.1.1. Synthetic HA

With the aim of synthesizing apatite nanocrystals, a protocol was carried out mostly according to the method described by Iafisco *et al*. [50], as the following:

- First thing before the start of the reaction, is the correct preparation of the reagents in use. To produce apatite with stoichiometric accuracy, a Ca/P ratio of 1.67 is desired. Thus, 2.62 g of calcium acetate hydrate [about 94% $Ca(CH_3CHOO)_2$] for soil testing, provided by Merck KGaA (1.09325.0500) were weighted in an analytical balance and successively dissolved with water in a beaker making up a final volume of 100mL. In parallel, inside the hood this time, 2.02 mL of concentrated H_3PO_4 (about 85-87 % wt/wt) were pipetted onto another beaker, and diluted with water until de final volume reached was 100mL.

  These preparations resulted in concentrations of 166mM and 100mM for $Ca(CH_3CHOO)_2$ and H_3PO_4, respectively.
- After the preparation of each solution, resembling a precipitation titration, the H_3PO_4 solution was poured into a burette, while closed, and the beaker with the dissolved $Ca(CH_3CHOO)_2$ was placed under it. A magnetic stirrer was also present below the beaker, and a magnetic stir bar inside, to facilitate the reaction.

- Once everything was in place, the reaction began with the slow addition of the phosphoric acid. To prevent the formation of other phosphates, the pH level had to be maintained at a level of around 10 with the addition of a few drops of concentrated $(NH_4)OH$ (about 28-30 % wt/wt) diluted at a 1:10 ratio. pH was monitored using pH stripes.
- After all the phosphoric acid was added, the solution was kept stirring at a low rate (about 300rpm) for 24h with occasional pH checks during that period. It was also left heated, ideally at 37ºC to optimize yield production.
- One hour before the 24h mark, the stirring was interrupted as well as the heating, allowing the deposition of the inorganic material in the bottom of the beaker.
- Subsequently the supernatant was removed and discarded accordingly and the jelly-like material in the bottom was equally distributed in 50mL falcon tubes.
- The following step was to centrifuge and allow the separation of the preferred material even further. After this procedure the solution was washed with water and centrifuged again.

  This step was repeated until the pH of the solution was at level 7 which was generally reached after roughly 4 times.
- To dry the solution completely, it was put in the stove at 60ºC for at least 48 hours.
- Finally, to finish this procedure, since the HA crystals dried in clusters of about 5mm, they were manually grinded using a pestle and a mortar.

In the rest of the text, we refer to this synthetic HA with the acronym SYN_HA.

2.1.1.2. Natural HA

In order to obtain natural hydroxyapatite nanocrystals, dry tuna fish bones were used, supplied by Mare Aperto SpA (Genova, Italia). To extract HA the following protocole was employed, based on that from Piccirillo:

- As soon as the shipment of tuna fish bones was received, a cleanse to remove fish remains was done, manually, so that mainly the bone itself was left (some small meat residues may still be present).
- Afterwards, the bones were broken into smaller pieces, and placed into calcination crucibles that withstand very high temperatures. This characteristic is important because of the next step.

- The crucibles with the fish bones were then put inside a muffle furnace at 700ºC. The temperature was increased at a rate of 5 ºC/min, until 700ºC, where it stayed for another hour.
- The machine was then turned off and left too cool down for 24h.
- The resulting fish bones were fully calcinated with a white, fragile appearance.
- The next step, identical to the final steps of the synthetization of HA, was to manually grind the samples until it looked like a fine, homogeneous powder.

In the rest of the text, we refer to this natural HA with the acronym NAT_HA.

However, since with the manual grinding there were still relatively large and irregular particles, both natural and synthetic HA particles were also treated by a mechanical milling, using a SFM-8 Agatemortar Grinder (MTI Corporation, Richmond, CA, USA) (**Figure 2.1** - left) after the manual process. This tools mortar and height adjustable pestle were designed for efficient, easy and uniform grinding. To start a cycle, 10g of HA powder, which was the ideal amount for the most efficient grinding cycle, were put onto the grinding mortar, followed by the addition of isopropanol, the added volume would have been enough to cover all the powder. Isopropanol worked as a solvent to ease the crushing and since it evaporated the sample composition wouldn't be compromised. With the automated controller a speed of 90rpm and timer for 180 minutes were set. During the procedure, solvent was added when needed to replenish the evaporated portion. In the end, the mixture was put in a large petri dish and left inside the oven at 60ºC to dry for 24h approximately. In the end, the result was a fine powder of hydroxyapatite, as desired.

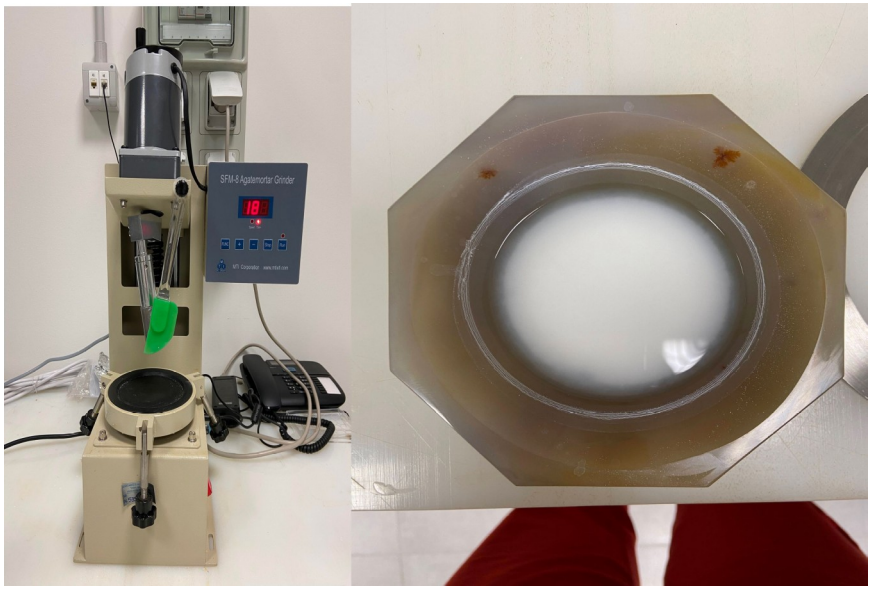

Figure 2.1 *(left) SFM-8 Agatemortar Grinder used (right) mortar with HA powder in isopropanol before grinding.*

2.1.2 Synthesis of Gelatin Methacryloyl (GelMA)

GelMA is a semi synthetic hydrogel formed by the combination of derivatized Gelatin with methacrylamide and methacrylate groups. Although the Gelatin has unique gelling properties, its low melting point makes it unsuitable for any biomedical application as a solo component. This is why its modification with methacryamide groups made a much more interesting concept since the resulting biomaterials became photosensitive and chemically stable, thus making good candidates for several tissue engineering adversities. The crosslinking of this material though is not temperature dependent so in order to solidify the hydrogel a photoinitiator agent is added. This means that the linking of the polymeric chains will only occur after its exposure to ultraviolet radiation, making it UV sensitive.

As for the methacrylation of the Gelatin, the subsequent protocol was followed, based on the general method firstly used by Van Den Bulcke et al[51]:

- First, 10g of Gelatin Porcine skin, type B, provided by Sigma Aldrich® company (G9391-100G) were weighted in an analytical balance and dissolved in a beaker at 10% w/v with phosphate-buffered saline (PBS; pH = 7.4) until the final volume reached 100 mL.
- To help the dissolution, the mixture was heated at 60 ºC and left stirring in a low rotation speed (about 100 rpm) for about 1 hour, covered with foil. This made sure that the Gelatin fully melted. Since a relatively clear solution should be the result, it was easy to spot any unmelted residues.
- The next step involved the careful and slow addition of 8 mL of Methacrylic Anhydride (MAA), also provided by Sigma Aldrich® company (276685 – 100 mL) using a 1000 µL pipette and letting the solution stir at 60ºC for 3 hours.
- 1 hour before the 3-hour mark, 400 mL of PBS, were preheated until the temperature reached around 40-50ºC.
- Once the 3 hours were complete, the reaction was interrupted and the heated PBS added to the mixture, diluting the GelMA at a 1:5 ratio and thus, topping the final volume at 500 mL.
- The mixture was then left stirring for an additional 15 min under the set temperature of 60ºC as mentioned earlier.
- Meanwhile, the molecular porous membranes (Spectra/Por molecular porous membrane tubing, 12-14 kDa molecular weight cutoff, Fisher Scientific) were cut in proper sizes of about 15 cm in length to be used in the dialysis of the GelMa. To

facilitate its opening, the membranes were placed into distilled water first, then a knot was tied in one of its ends.

- After this the diluted GelMa was poured inside and another knot was tied on the other end to close it inside. The amount left was enough to repeat this procedure 4 more times.
- Each sausage-shaped GelMA membrane was then placed in a 5L beaker full of distilled water, where it stayed floating vertically at 40-50 ºC, stirring at about 300 rpm for about 1 week allowing the dialysis reaction to occur. The water was changed at minimum 2 times a day every day and each time the membranes were reversed, so the toxic unreacted methacrylic anhydride is removed from the GelMA.
- On the 8th day, the dialysis was stopped and the GelMA was filtered using a sterilized filter. The product of this was then transferred into 50 mL Falcons (with 25/30 mL each). Later on, they were stored at -80ºC for at least 2 days in the fridge.
- The final step, was to lyophilize the frozen GelMA in a freeze-dryer (Lio 5P) for at least 2 days. In this process, the water from the product placed under vacuum, in this case GelMA, is removed by allowing the ice to transition directly from its solid state to vapor (sublimation), without passing through the liquid stage.
- By the end a foamy material was the result and stored at 4ºC.

2.2. Hydrogel preparation/optimization

2.2.1. GelMA-HA-LAP based hydrogel preparation

The preparation of GelMA-HA-LAP based hydrogels was carried out according to the protocol described below. This process depicts the preparation of 3 mL of sterile GelMA solution at 10% (wt/vol) in PBS, with LAP photoinitiator at a concentration of 0.5% (wt/vol) and synthetic hydroxyapatite nanocrystals at a concentration of 1% (wt/vol). All the following steps were conducted under sterile conditions inside the hood (Bioair Safe Mate Eco^{+}) as described more in depth:

- A day prior to the intended time of preparation of the hydrogels, the sterilization of hydroxyapatite had to be done. For that, 30 mg of synthetic HA powder were weighted and placed in a sealed Eppendorf and placed in the oven at 100ºC for 12 hours.
- Before mixing, both GelMA and the HA, plus a magnetic bar, a beaker, polydimethylsiloxane (PDMS) molds and a spatula were sterilized under UV light inside the hood for 30 minutes.

- Next step, it was to place the sterile GelMA in the glass beaker and heat it at approximately 60ºC while simultaneously adding 3 mL of sterile PBS, sealing it with parafilm in the end to prevent water evaporation. The solution was left to dissolve for about 30 minutes, with the help of a magnetic bar with very slow rpm to avoid the formation of bubbles.
- Then, after it had been dissolved completely, the HA was added and kept stirring for 15 minutes more. The HA is not soluble but some time is given for it to disperse uniformly in the solution before the addition of the final component.
- Finally, 15 mg of LAP photoinitiator were weighted in a plastic weighting boat and right after added to the solution. The beaker was immediately covered in tinfoil to protect from light, as the photoinitiator made the solution light sensitive, to avoid its premature crosslinking.

  As before, the mixture was kept stirring at 60ºC until it was clearly homogenous.
- The GelMA-HA-LAP solution was then poured into a PDMS mold, a rectangular shaped mold with three wells, each with a diameter of 8 mm and a height of 4 mm.

  These molds are used to give shape for the hydrogel, allowing replication for further testing on the hydrogel properties.
- The samples were then placed under UV light at 365nm in a specific UV curing oven (marketed by Asiga®) for 60 seconds. During this time, crosslinking happens, hardening the samples allowing the sol-gel transition to take place.
- In the end, with the help of a spatula, the crosslinked hydrogels were removed from the PDMS molds.

2.2.2. Chitosan-HA based hydrogel preparation

The chitosan-based hydrogel is quite different from the one previously described. It is a thermosensitive hydrogel which can undergo a sol–gel transition as the temperature increases. According to the protocol described by Stanzione et al. [38], for the preparation of this hydrogel, a combination of chitosan and β-glycerophosphate (BGP) in the right ratio would allow the sol-gel transition at 37ºC. In summary:

- To prepare a substantial amount of both Ch and BGP for multiple tests, 3.33 g of low molecular weight Ch powder (degree of deacetylation 75–85%, MW 50.000–190.000 Da, #448869, Sigma Aldrich, Milan, Italy) were weighted and solubilized at 3.33% (w/v) with 100 mL of 0.1 M HCl in a beaker.

- Afterwards, the solution was left stirring at a low rate (300rpm) overnight at room temperature (~20ºC).
- Next step was to centrifuge the solution at 2500 rpm for 5 minutes. This step would remove all air bubbles created during the stirring part.
- Setting the Ch solution aside after it was finished and placing it in the fridge at 4ºC, the preparation now focused on dissolving βGP salt pentahydrate powder (MW 306.11 g mol−1 , #35675, Sigma Aldrich, Milan, Italy) in 10 mL of distilled water.
- In the end both compounds were placed in the fridge at 4ºC until further use.

When creating the chitosan-BGP-based hydrogel, the final ratio (v/v) in solution between Ch and BGP was 3:2, respectively. This equilibrium ensured the polymerization of the hydrogel at 37ºC. In this case, to prepare 3 mL, final volume, of hydrogel solution, the following steps were respected:

- With the help of a 1 mL syringe, 1.8 mL of Ch were placed in a small glass vial. Since the Ch has a thick texture the syringe was the best way to transport the amount needed.
- Next, with the help of a pipette, 1.2 mL of BGP were added to the vial. All these steps were immediately followed by the placement of the vial in ice, to avoid any premature polymerization due to the higher room temperature.
- Right after the addition of BGP, with the help of a spatula, the substances were mixed very well until a homogenous solution resulted.
- 200µL of Ch-BGP solution was then poured into each well of a PDMS multi well plate (**Figure 2.2**), like described above (three wells, each with a diameter of 8 mm and a 4 mm height).
- The samples were then placed inside the oven at 60ºC and left for two hours to complete the polymerization process, during of which the sol-gel transition occurred.
- In the end, with the help of a spatula, the hydrogels were removed from the PDMS molds.

The addition of hydroxyapatite to this process changed some of the steps mentioned above. Several tests were made in order to find the optimal combination of the components. Different concentrations of HA were tried, with both synthetic and natural HA, ranging from 0.125% to 1% w/v as shown in **Table 2.1**.

Table 2.1 *Concentrations of tested HA incorporated in the Ch-based hydrogel.*

Concentrations of HA incorporated and tested in the Ch-based hydrogel (w/v)							
	pH	**Homogeneity**	**Inject.**	**Polym.**	**Stability test**	**Compression test**	**Bioprinter**
Synthetic	0.125, 0.25 and 0.5%	0.125, 0.25, 0.5, 0.65, 0.7, 0.8, 0.9 and 1%	0.125, 0.25, 0.5, 0.7 and 1%	0.125, 0.25, 0.5, 0.7 and 1%	0.125, 0.25 and 0.7%	0.125 and 0.25%	0.125, 0.25, 0.5 and 1%
Natural	0.125 and 0.25%	0.125, 0.25, 0.5, 0.7 and 1%	0.125, 0.25, 0.5, 0.7 and 1%	0.125, 0.25, 0.5 and 0.7%	0.7%	-	0.125 and 0.25%

The order in which HA was added was also subject to testing. In the end, the best hydrogel/bioink creating process came down to two concentrations as the higher ones were not explored further because the hydrogels did not have good properties. Those concentrations were 0.125% and 0.25% (wt/vol) of HA (for a final volume of 3mL that meant that in each solution, 3.75 mg and 7.5 mg were used, accordingly). As example, the 0.125% (wt/vol) solution is described below.

- First things first, a regular sieve with holes with the size of about 4x4 mm was used to sieve the synthetic HA (previously mechanically grinded twice). This resulted in the bigger particles being retained and separated.
- After different tests, it was seen that the best way to incorporate the HA was to mix it with BGP first and separately from the Ch. Therefore, 3.75mg of synthetic HA were weighted and placed in a vial.
- Next, with a pipette, 1.2 mL of BGP were added to the glass vial, and taken to the sonicator for a process called sonication bath. A timer was set to 5 minutes at a frequency of 5 kHz.

The sonication process is very important for the deagglomeration of nanoparticles, and dispersion, all very common problems when working with HA. Through sound energy, the particles are agitated and thus separated.[52]

- After this, to ensure homogeneity, the vial was taken to the vortex for 30 seconds.
- In the end, 1.8 mL of Ch were then added and the vial placed in ice.
- The rest of the protocol follows the same steps as with the Ch-BGP-based hydrogel described above.

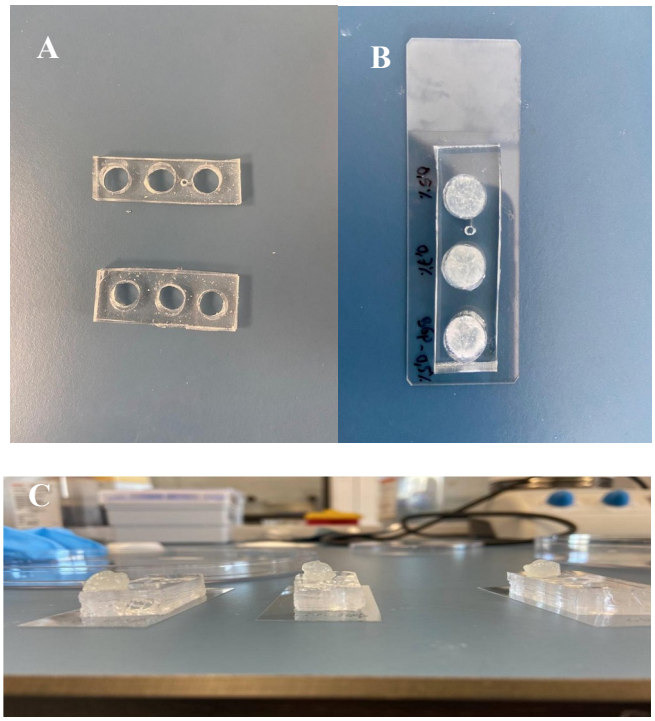

Figure 2.2 *Schematic representation of hydrogel formation: (A) PDMS molds used (B) PDMS molds with solution pre-polymerization and (C) Hydrogels formed after polymerization.*

2.3. Characterization

2.3.1 HA nanoparticles

For a possible future application in bone regeneration, the role the size of HA nanoparticles has, will have a great effect on bone cell proliferation.

With that being said, some tests were performed in order to characterize natural and synthetic HA.

2.3.1.1. X-ray Diffraction (XRD)

X-ray Diffraction analysis is a commonly used technique when to determine its phase composition, i.e. the nature of the chemical compound(s) the material is made of. In fact, it

gives information regarding the crystallographic structure, chemical composition and physical properties of the material in question.

Hence, with the purpose to acquire and compare such data on synthetic and natural HA, both samples were analyzed with an X-ray diffractometer (X'Pert PRO MRD, Malvern Panalytical LTD, Malvern, UK).

To prepare the samples for XRD, with the help of a small spatula a small amount of each was placed in the center of a glass slide. Since the glass slide would have to be in a vertical position, the samples were fixed to the glass by applying a drop of isopropanol on its surface and allowing it to dry out. Since the isopropanol evaporated it would not compromise their structure.

When taken to the XRD machine, one of the glass slides was carefully placed inside vertically with the help of some metal supports. The procedure itself looks rather simple: the sample is hit with a beam of X-rays and the refracted signal is then detected by a Detector. The information is then translated in a graph with a specific number of peaks with specific values according to the material in question. The important part though, happens in the atomic level. X-rays are high-energy light with a repeating period called wavelength (λ). Since the λ of an X-ray has a value comparable to the distance (d) between the different atoms, a process called "diffraction" can be used to measure that distance. For this to happen, no interference between the x-ray waves can happen, they must be aligned in what is called "constructive interference" (**Figure 2.3**). This will allow the amplification of the signal translated into peaks. Now in a crystal, when the atomic planes are exposed to an x-ray beam, x-rays are scattered by the regularly spaced atoms. However, strong amplification of the emitted signal occurs at very specific angles (θ) where the elastically scattered wave constructively interferes. This is called "diffraction".

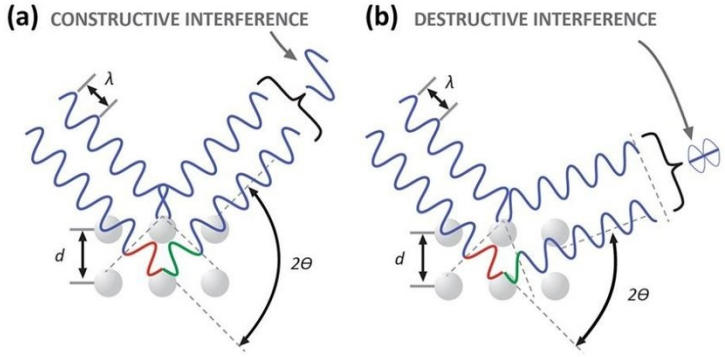

Figure 2.3 *(a) Constructive Interference (b) Destructive Interference* [53]

When the incident angle produces waves that constructively interfere, the Bragg´s Law applies:

$$2d\sin\theta = \lambda$$

In the equation, λ is the wavelength of the incident beam (fixed and known), q is the value of the diffraction angle (measured) and d is the distance between the atoms, which can be calculated. This can give information about the crystallographic structure of the analyzed material. [53]

For this procedure, the X-ray diffractometer used a Cu K-α radiation with λ equal to 15.41 nm, generated at 40 kV and 40 mA. The 2θ range was from 10º to 60º with a step size (2θ) of 0.005º and a counting time of 100 s.

To determine the sample composition, the acquired diffraction pattern was compared with the standard HA diffraction pattern (reference file 01-072-1234 of the database).

2.3.1.2. Scanning electron microscopy (SEM) analysis

With the intend to assess and compare the size of the nanoparticles of synthetic and natural HA, samples of each were observed by the scanning electron microscope (SEM EVO 40, Carl Zeiss AG, Oberkochen, Germany).

SEM is a widely used instrument for the physical characterization of solid materials. It offers a close image of the samples surface allowing the analysis of its microstructure and morphology. Its working principle is simple, the images obtained are a result of the emission of an electron beam that scans the surface of the material. When the resulting signal from the electron-sample interaction returns, it will be detected and then an image will be formed.[54]

During a SEM test the samples are bombarded with high-energy electrons; if the samples are not conductive, this will result in a build-up of negative charges. This can create noise in the signal, negatively influencing the obtained image. As hydroxyapatite does not conduct electricity (it is insulating), an additional step had to be performed to avoid this problem; the sample, in fact, were coated in a thin layer of about 10 nm of a conductive material, in this case gold. The preparation of the samples was a very simples process: two different pieces of two-sided conductive carbon adhesive tape were place on top of two different SEM metal stubs, and then a small amount of each of the HA nanocrystals was placed on top of the conductive tape.

The samples were then covered with a layer of gold using a Compact Coating Unit-010 (Safematic GmbH, Zizers, Switzerland) (**Figure 2.4**). The gold coat acts as a channel

allowing the build-up of charging electrons to be removed and thus creating a clearer image. [54], [55]

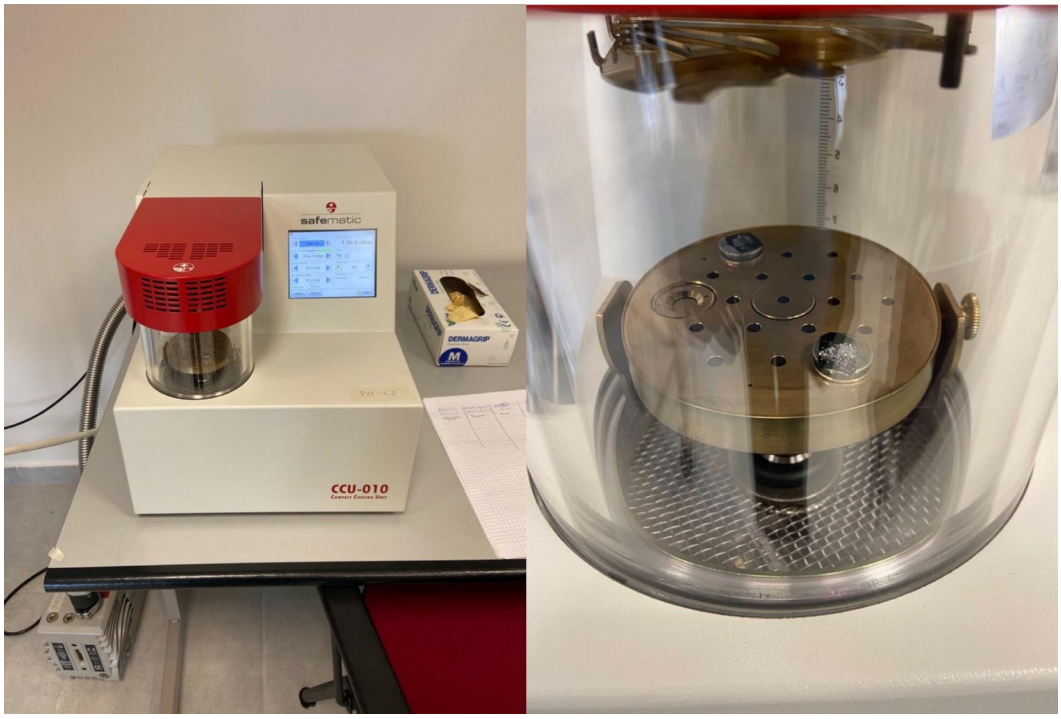

Figure 2.4 *(left) Compact Coating Unit-010 (safematic GmbH) for HA particles metallization, (right) HA particles being coated.*

After this process, the gold coated samples were then placed in the SEM machine and were ready to start. Images with different magnifications were acquired during the procedure as it was directly related to the Work Distance (WD). This means that in order to obtain the best image the correlation between the final lens and the sample in focus had to be ideal. In other words, the lower the WD the higher the magnification.

2.3.2 Chitosan-HA hydrogel characterization

To evaluate the physical, chemical and mechanical properties of the Ch-HA based hydrogel several tests were conducted and described below.

2.3.2.1 pH homogeneity and polymerization

Hydrogels with natural and synthetic HA were tested at the defined concentrations of 0.125% and 0.25% each.

The pH of each hydrogel was also tested. The final goal of these materials will be to implement them with cells in the human body, so the pH must answer their requirements. This would mean that it should be at a level of around 7.

Right after the preparation of the solutions, while cold, a pH test strip was placed in the material with the help of a clamp. After a few seconds of contact with the material, the strip was removed and the color was interpreted.

To test the polymerization, samples prepared according to Ch-HA hydrogel protocol were placed in the oven at 37ºC, where they were left for 2 hours. In the end, and with help of a spatula, the formed hydrogels were removed from the molds. Shape, size and stiffness were monitored as preliminary parameters to evaluate the successful polymerization.

The shape and size of the hydrogel were visually assessed and the stiffness was tested by a manual compression. The stiffness was later on thoroughly analyzed by compression test.

2.3.3.2 Stability test

Stability tests were performed in order to evaluate the hydrogel degradation under physiological conditions in a controlled *in vitro* environment. These tests allow to understand for how long the material will remain safe and effective.

As described previously, after the preparation of the hydrogel solutions, 200 µL were transferred into each well of the PDMS plates, making three replicates. Then they were placed inside the oven at 37ºC for 2 hours. Polymerization occurred during this process. After this time, with the help of a spatula the polymerized cylinder-shaped hydrogels were removed from the molds and weighed (W_0). They were then placed in each well of a 24 well plate and immersed in PBS. The degradation profile was measured with the weights of each sample at different timepoints. Including the measurement before PBS immersion which accounts for time zero, the others were taken at 1 and 24h and 3,7 and 10 days after. During each individual measurement, before being weighted, each sample was dried in absorbent paper to remove excess PBS. The percentage of weight loss (WL) was calculated according to the equation [38]:

$$WL(\%) = \frac{W_0 - W_i}{W_0} \times 100$$

where W_i stands for the weight collected at different selected timestamps.

2.3.3.3 Compression test

Compression tests were performed on Ch and Ch-HA hydrogel in order to evaluate if the presence of HA modifies the hydrogel stiffness. A stress-strain test was carried out in triplicate

on each sample. [56]

Samples were prepared as described above. The samples were assessed at room temperature in wet conditions (submersed in PBS). For the performance of the test, a universal testing machine (ZwickiLine 1kN, Zwick Roell, Kennesaw, GA, USA) equipped with a 10N cell load was used.

The mechanical properties of the Ch and Ch-HA based hydrogels were measured with uniaxial compression tests, in displacement control at a rate of 2 mm/min up to 75 % of the strain. Samples with dimensions of 9.5 mm in diameter and about 4 mm in thickness were used. Three replicates for each hydrogel formulation were tested in wet conditions. In order to evaluate the stiffness of the Ch-HA hydrogels with the two HA loads (0.125 and 0.25% w/v), the stress was plotted as function of strain and the Young modulus was calculated as the slope of the linear region of the curve (i.e. in the strain range 0 – 5%). Pure chitosan hydrogel was also tested as control.

E, described as the ratio of stress to strain, was obtained in accordance with the equation:

$$E = \frac{\sigma}{\varepsilon}$$

where σ represents the stress and ε represents the strain.

2.4. 3D Bioprinting

2.4.1 Bioink printability

All the former tests presented allowed the study of mechanical, physical and chemical properties of the Ch-HA hydrogel. Successively its behavior as a possible bioink had also to be assessed.

For this, as a first screening, a preliminary manual printability test was performed (**Figure 2.5**). This test is conducted immediately after the making of the hydrogel solution, but before its polymerization. It permitted the analysis of the material's ability to form fibers rather than droplets, as well as the fibers' capacity to stack layer by layer to create 3D constructions without merging. A protocol as described by Paxton et al. [57] was followed.

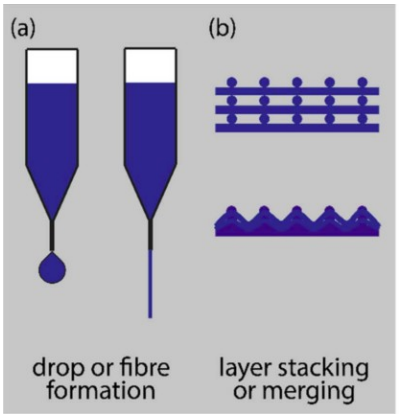

Figure 2.5 *Initial screening of ink formulation to establish (a) fiber formulation as opposed to droplet formation and (b) successful layer stacking without merging between layers (image from Paxton et al. [12]).*

As described above (paragraph **2.2.2.)** right after the preparation of the hydrogel solution, while it was still in a gel-like state (at 20°C), 1 mL of solution was loaded into a 1 mL syringe equipped with a 0.44 mm (25G) conic needle. Afterwards, a manual dispensing was applied to evaluate the hydrogel injectability. The material was extruded at a constant pressure to assess whether the hydrogel flowed continuously from the syringe in the form of fiber and / or if there were any obstructions caused by HA particles/clusters. Hydrogels with natural and synthetic HA were tested at the defined concentrations of 0.125% wt/vol and 0.25% wt/vol each.

2.4.2 Preprinting hydrogel conditions

The most important aspect about the Ch-HA based hydrogel is that it is thermosensitive. According to the data reported by Stanzione et al. [38], related to the rheological and compressive properties of Ch-BGP hydrogels the temperature at which it undergoes the sol-gel transition happens is 37ºC. Extrapolating with the case of our hydrogel, which contains hydroxyapatite nanocrystals, since the HA doesn't present thermosensitivity, it is believed that it won't change the sol-gel transition point. Although it is worth mentioning, that the addition of HA improved mechanical properties as well as viscoelastic properties, as demonstrated in a study by Kumar et al. [58]. This means that, it may polymerize faster or at least appear more viscous than a chitosan hydrogel at the same temperature. Extra steps must be taken to prevent this, as the ideal stat of the hydrogel should be somewhere between liquid and gel-like. In fact, if it were in a liquid condition, the three-dimensional structure would

collapse and lose its ability to take on the proper form. If it were in a gel state, it may also clog the nozzle in addition to requiring increased pressure to extrude.

Knowing this, to ensure a good printing trial, Ch-HA hydrogel solution after being prepared is transferred into the extruded syringe used in the 3D bioprinter and cooled in ice until the temperature of 20 ºC has been reached. This will prevent premature polymerization as it can be triggered by the room temperature if warm enough.

2.4.3 3D bioprinter and cartridge set up

The 3D bioprinter used during this experience was the R-GEN 200 model (Regen HU®, Switzerland), as shown in **Figure 2.6**.

R-GEN 200™ is an extrusion-based bioprinter, which pressures the biomaterial ink or bioink out of a nozzle with the aim to create three-dimensional structures. In order to do that, R-GEN 200 is equipped with an *air compressor* with pressures between 6 - 10 bars to power the tool changer as well as to send the material flow from the cartridges to the printhead. The compressed air is delivered to the *four dispensing tools*: PSD, PDD, PMD and VSD.

Figure 2.6 *R-GEN 200 3D bioprinter station (REGENHU® company)*

- The Pneumatic Strand Dispenser (PSD) is a sterility-focused direct pressure print head, dedicated for use with highly viscous media, such as pastes or gels.

- The Pneumatic Drop Dispenser (PDD) dispensing tool is a valve based low to mid viscous media printhead. It can be used for contact dispensing as well as for jetting.
- The Pneumatic Melt Dispenser (PMD) printhead is mainly designed to dispense high-temperature (melting point up to 250°C) thermoplastics. It can be also used for any paste or gel like materials that are compatible.
- The Volumetric Strand Dispenser (VSD) printhead is dedicated to volumetric dispensing, allowing a constant flow of defined material quantities largely

independent of material viscosity. It can be used with media with low to high viscosities, such a liquids, gels, or pastes.

This bioprinter is also equipped with a *light curing kit* (LCK). It contains two different LED based point sources with emitting wavelengths of 354 nm and 405 nm. This specific characteristic is very useful and interesting if the material used is photosensitive as the monochromatic spectrum matches the absorption of photoinitiators in these UV curable materials. This translates to crosslinking of the material. R-GEN HU is also able to perform needle calibration with the help of a *needle calibration sensor* (**Figure 2.7**). It is used to measure the length of the printhead needle tip and a possible offset in the X and Y axis caused by a deformation of the needle tip. For the bioprinting of bioinks a special instrument was incorporated called the *cell agitator*. The cell agitator is designed to prevent cell sedimentation and assure cell and particle homogeneity during the printing process. It is applicable on Pneumatic Drop Dispenser (PDD) and Pneumatic Strand Dispenser (PSD) only.

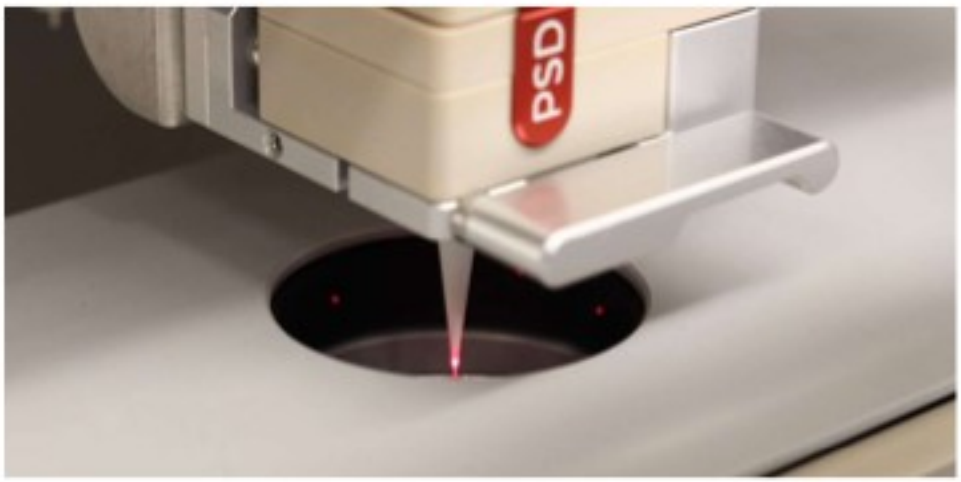

Figure 2.7 *Needle calibration sensor of the PSD printhead tool.*

The 3D bioconstructs may be printed on various *substrates* (for example, glass slides, Petri dishes, and multi-well plates) and then put on the desired workzone. In fact, each material works best in a specific workzone based on the temperature control requirements and the bioprinting procedures utilized. The *workzones* available for this bioprinter model are the Eletrospinning and Writing Kit (ESK) and the Physiological Temperature Workzone Kit (WTP).

- The combination of printhead and ESK Workzone enables the instrument to perform melt-electro-writing and solution-electro-spinning technique. In melt-electro-writing mode, the ESK Workzone is combined with the PMD tool. In solution-based electrospinning mode, the ESK Workzone is combined with the VSD tool. To draw the fiber from the spinneret to the collector plate by the means of an electrical field a maximum voltage of -25kV can be applied to the ESK Workzone.
- The WTP allows printing thermosensitive hydrogel precursors. It's ideal for printing of cell-laden materials at physiological temperature (37°C) ranging from 5ºC to 40ºC.

Workzones are protected by the platform cover which is equipped with *6 cleaning stations* and *2 purging stations* (**Figure 2.8**). A cleaning station for the needle tip is supplied for each printing instrument. There is no chance of cross contamination because each head has its own station. At the end of the printing process, two purging stations are available to dispose of your surplus biomaterial within disposable bins.

Figure 2.8 *Platform cover of Workzone. It's possible to see the cleaning and purging stations, and the workzone where a well plate was fixated.*

At last but definitely not least, the bioprinter has its own *design software* and *control software*: SHAPER and R-GEN Controller, correspondingly. The REGENHU R-GEN Controller software is the human and machine interface program used to monitor the condition of the R-GEN bio printer, print the files provided by SHAPER, and operate the R-GEN printers directly. SHAPER is used to develop, alter, and PLACE the required item or

structure to be printed. It allows you to simply design your 2D and 3D structures or import them from another source.

The PSD printhead (**Figure 2.9**) was the one chosen for this work given to the fact that the Ch-HA hydrogel, possesses high viscosity below 25°C. Indeed, the PSD printhead permitted the testing of a wide variety of pressures to determine which was optimum for the Ch-HA hydrogel. But before, the proper bioprinter setup, including cartridge loading and optimal printer settings were studied, resulting in the fabrication of 3D biological constructs with the best viability and quality.

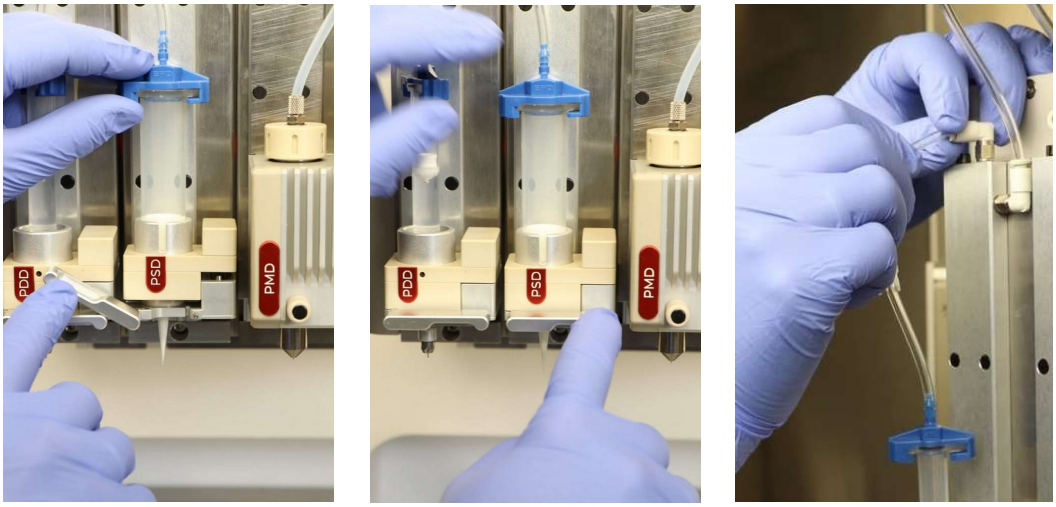

Figure 2.9 *PSD cartridge installation and pneumatic pipe connection.*

The cartridge loading was conducted following these steps:

- Initially, the PSD cartridge was loaded with the hydrogel through a Luer Lock connector. It had been in ice right before this process. The cartridge was loaded upside down to avoid causing or adding air bubbles inside the hydrogel.
- the Luer Lock connector was then replaced with the conic 25G needle.
- Lastly, the cartridge was put into the PSD printhead. The cartridge was fitted into the printhead's selected cartridge adapter by pushing it down until it was fully inserted. The pressure adaptor was then placed over the cartridge.

As previously stated, it is fundamental to maintain the cartridge temperature at 20°C to prevent the hydrogel polymerization inside the cartridge which would make it unsuitable for printing.

2.4.4 Structure design and optimization of bioprinting parameters

A research was conducted in this section of the work to determine the optimal bioprinting parameters for the Ch-HA hydrogel, with synthetic HA only. Different pressure settings (12 - 30 kPa) were tested to determine which was optimal for efficient and reliable 3D printing. Then, with the help of the R-GEN 200 bioprinter and a conic microextrusion 25G needle, the bioprinted objects were created.

The initial stage was to create a computer-aided design model (CAD) that could be used for bioprinting. In the "designer" area of the RegenHU ShaperTM program, a pattern of three lines, each 10 mm long and separated by 2 mm, was created. This structure was cloned twice to test three different pressure levels.

The intended shape was modified to print on a glass slide, which served as the bioprinting substrate. Each group of three lines was placed on the glass slide using the Shaper software's "composer" function (**Figure 2.10**).

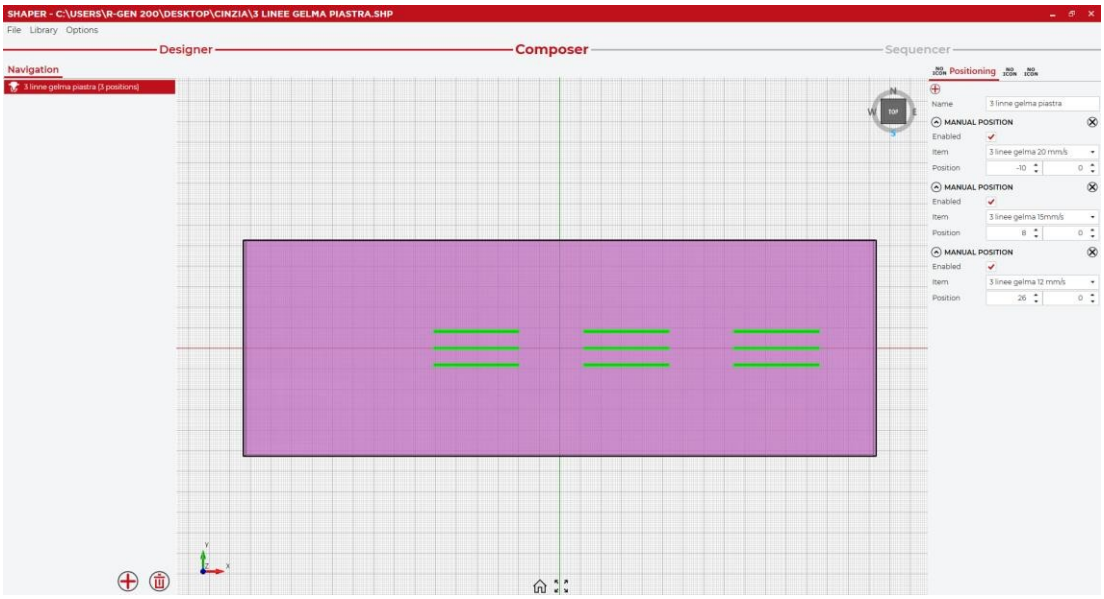

Figure 2.10 *Manual position of the designed geometry on the glass slide.*

The bioprinting technique included a single layer deposition at tested robot speeds between 2-12 mm/s with a needle offset to the substrate of 0.1 mm. Each line's strand height and strand width were both 0.41 mm, the same measurement as needle diameter.

The biofile, generated using Shaper software, was then 3D printed. To do this, the Controller program was used (**Figure 2.11**), which allowed to monitor the R-GEN bio printer's status, print Shaper files, and directly manage the R-GEN printer. The chosen

cartridge was PSD (Pneumatic Strand Dispenser) and the workzone was WTP (Physiological Temperature Workzone).

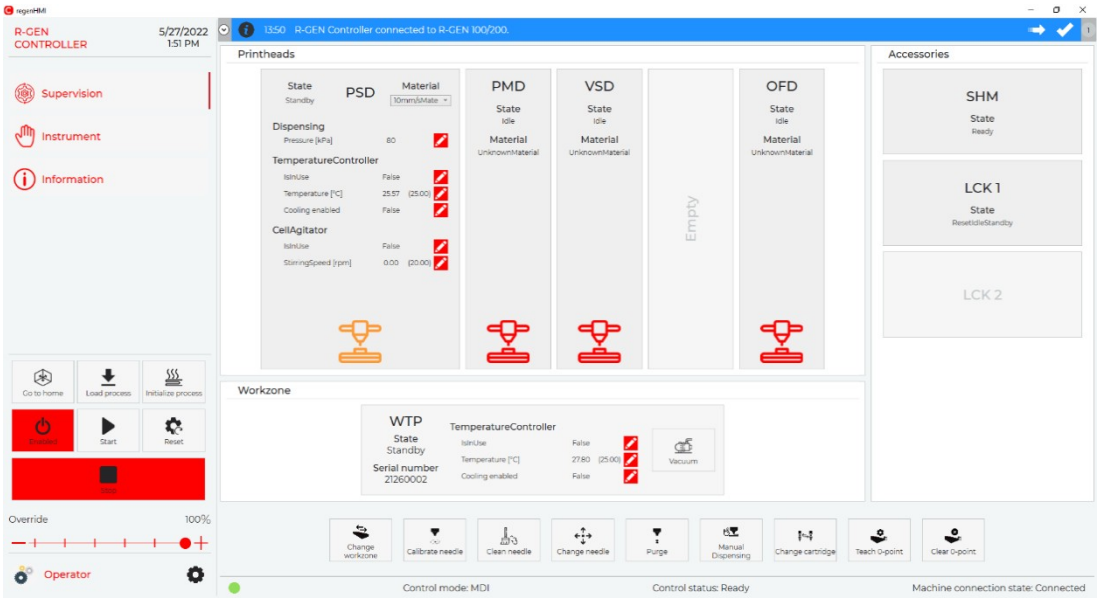

Figure 2.11 *Controller Software, by RegenHU.*

After configuring the test settings, the Ch-HA hydrogel was produced and placed into the bioprinting PSD cartridge, as previously mentioned. The automated needle calibration was completed, and the bioprinting procedure began.

The thickness of each line was measured after printing to determine the ideal printing pressure for the Ch-HA hydrogel. Pictures of the 3D printed structures were acquired using a digital microscope, the Dino-Lite Edge PLUS 1.3MP, 10-14x. The images were then examined using ImageJ software. Three measurements were made on each line and the mean value was compared with the needle diameter (0.44 mm).

2.5 Statistical analysis

Results were expressed as a mean value ± standard deviation. Statistical analysis has been carried out by Student's T-test (Excel software) two tails, un-paired, to evaluate the significance of the data. The values were considered statistically significant with $p < 0.05$ (*).

3. RESULTS AND DISCUSSION

3.1. HA nanoparticles characterization

3.1.1 X-ray Diffraction (XRD)

The crystallinity and the composition of synthetic and natural hydroxyapatite nanocrystals were assessed using X-ray diffraction (XRD).

When studying the SYN_HA nanocrystals, as mentioned in the introduction, it was important to verify the purity of our samples. The formation of β-TCP can indicate that the Ca/P ratio is lower than 1.67. On the other hand, a Ca/P ratio higher than 1.67 can lead to the formation of other phosphate phases. With this X-ray Diffraction analysis, it is possible to verify the presence of such components.

In the following image (**Figure 3.1 top**), we can make a comparison between SYN_HA powder as prepared, synthetic HA calcinated at 700ºC and standard HA diffraction pattern (American Mineralogist Crystal Structure Database (http://rruff.geo.arizona.edu/AMS/amcsd.php). The SYN_HA as prepared shows large peaks, indicating low crystallinity level; this is reasonable, since it was prepared at relatively low temperature. With such large peaks, it was difficult to detect possible other phases such as b-TCP, as the signals would have overlapped and not being visible; because of this, the SYN_HA was calcined at 700 ºC. It's possible to see that the calcination process translates to sharper peaks. This indicates higher crystallinity by the nanocrystals. Comparing its diffraction pattern with the XRD values of standard HA (**Figure 3.1 bottom**) below the top graph, it can be seen that no other signal is present. This shows high purity levels of the prepared samples.

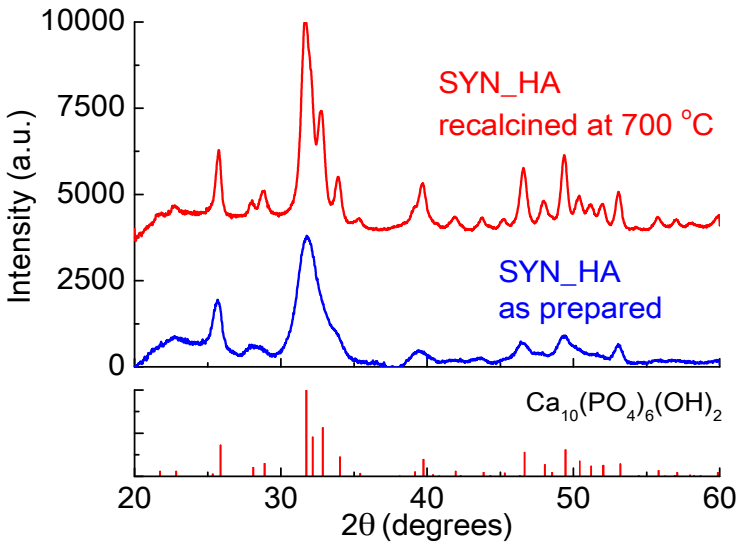

Figure 3.1 *XRD patterns for: (top) SYN_HA calcinated at 700ºC (red) and SYN_HA as prepared (blue); (bottom) standard HA values.*

Concerning the XRD analysis of natural hydroxyapatite (**Figure 3.2 top**), it's possible to see that it also contains very sharp peaks. Comparing it to the SYN_Hap, it could be said that NAT_HA has higher crystallinity as it shows a much sharper diffraction pattern. When comparing it with the graph of standard Hydroxyapatite values (**Figure 3.2 bottom**), it is possible to see a match again between all the peaks, with no signal of other compounds detected. This is an indication of a high level of purity, which means that there were no TCPs present or at least not in a significant amount.

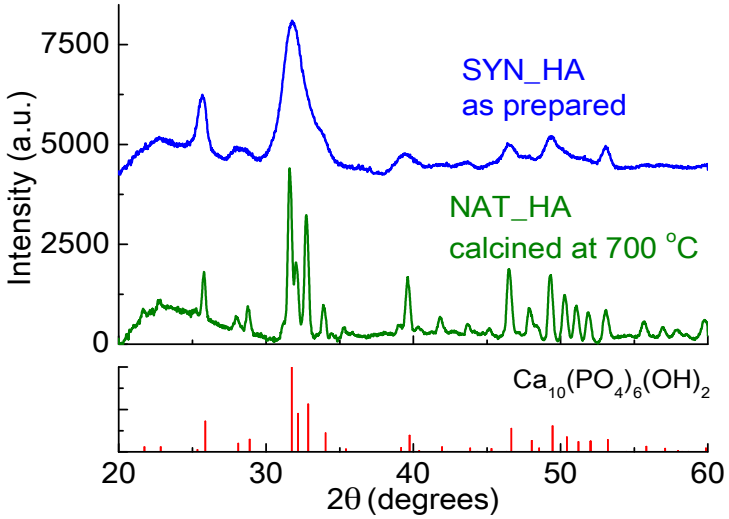

Figure 3.2 *XRD patterns of (top) SYN_HA as prepared (blue) and NAT_HA calcinated at 700ºC (green); (bottom) standard HA values.*

Since all the samples demonstrated high degrees of purity, according to the respective XRD patterns, they were all deemed fit for biomedical application but more importantly NAT_HA calcinated at 700ºC and SYN_HA as prepared.

3.1.2 Scanning electron microscopy (SEM)

Scanning electron microscopy analysis was carried out with the aim to evaluate the physical characteristics and differences between synthetic and natural hydroxyapatite nanocrystals.

Through the magnified images presented below (**Figure 3.3**), it's possible to see a clear distinction in both morphology and size. Images A and B correspond to NAT_HA nanocrystals. They can be described as long rod-shaped nanoparticles, with length between the 200-600 nm and width of about 30-50 nm. The particles are very similar between themselves morphologically, and gathered in clusters, the last one being a very typical characteristic for hydroxyapatite. Images C and D relate to SYN_HA nanocrystals. As it can be seen, the nano-sized crystals are very heterogeneous in size, not possessing a well-defined shape, as opposed to the natural ones. They also have a size range much smaller, having particles as small as 19 nm all the way up to 180 nm, which is still considerately smaller than the tiniest natural HA nanocrystal. Such difference in size may be due to the aggregation of the smaller particles into larger ones.

Studies suggest a dependency in the shape and size of the nanocrystals as an important factor for tissue regeneration. These characteristics influence cell growth and death. Some reports claim that small needle-shaped HA particles cause a longer inflammatory response than spherical shaped nanoparticles, indicating that these may be deleterious to effective tissue remodeling [59]; others reports, however, state the opposite [60]. Either way the shape of the particles is an important feature. According to Yurong et al.[61], smaller particles of about 20 nm have the greatest potential for stimulating bone regeneration and inhibiting the growth of osteosarcoma cells. When compared with bigger nanoparticles of 40 and 80 nm, the cell proliferation is also revealed as a lot higher, suggesting that the smaller the particle size the better its application in bone reconstruction/replacement.

When taking this into consideration, both kinds of HA will be tested for the hydrogel's preparation, although SYN_HA is probably more suitable, due to the smaller particle size.

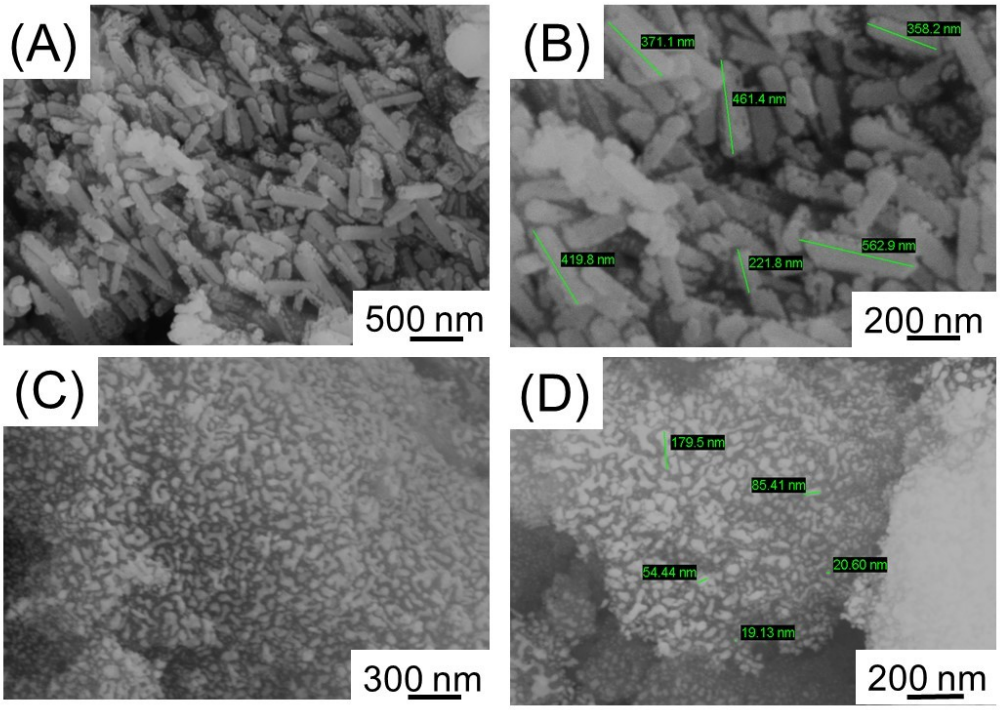

Figure 3.3 *SEM images of HA nanocrystals. (A) & (B) NAT_HA, (C) & (D) SYN_HA.*

3.2. Hydrogel characterization

3.2.1 GelMA-HA hydrogels

Due to its gelation properties and excellent solubility, biodegradability and biocompatibility it could be a very good base hydrogel for the addition of hydroxyapatite. Some test assessments like homogeneity, crosslinking and injectability were performed to test its compatibility with hydroxyapatite and they actually performed well, although the right concentration still hadn't been found. The problem with this material occurred when attempting to perform a stability test. Several stability tests were conducted but the material was not stable for more than 3 days. A contamination was thought to be the problem, but even when the solution was made in sterile conditions, the problem was not resolved.

Based on these results, no further tests were performed on these hydrogels and the work was focused on the Ch-HA hydrogels.

3.2.2 Ch-HA hydrogels

As mentioned in **table 2.1**, many HA concentrations were tested to understand which would be best in the Ch-based hydrogel. SYN_HA was tested first, due to its smaller particles size; what worked for the synthetic material was replicated with NAT_HA. The tests started from the highest concentrations and slowly decreased, as the concentrations showed to be too

high to obtain hydrogels with suitable properties. Concentrations above 0.25% (wt/vol) were tested for the bioprinting process (without some additional measurements); such tests were made to understand the performance of the material, sometimes using a needle size of 0.66mm. Once it was clear that the needle tip had to have a diameter of 0.41mm, then the concentrations of 0.125% and 0.25% (wt/vol) were the ones used for more tests (stability and compression).

3.2.3 pH, homogeneity and polymerization

As stated in the previous section, chitosan-HA hydrogels were prepared with HA concentrations of 0.125 and 0.25 wt/vol % HA. In order to further comprehend the characteristics of the hydrogels, three characteristics were analyzed: pH, homogeneity and polymerization.

Table 3.1 shows the results of these tests that allowed the comprehension in behavior of each sample. Ch-BGP hydrogel composition has already fine-tuned in the protocol of Stanzione et al[38]. The pH test was performed on Ch-HA hydrogel to verify that the addition of hydroxyapatite did not change the pH and that therefore the hydroxyapatite does not solubilize during the process. Next test included the evaluation of the homogeneity of the mixture. It is important that the HA nanocrystals are disposed in a homogenous matter. The results indicated that the most visually homogenous solution was the one with 0.125% wt/vol concentration of SYN_HA. The other samples either demonstrated some traces of heterogeneity or did not react at all and did not mix. The polymerization process was evaluated simply by visualizing if all the material had solidified and if it was of a strong consistency. The material was squashed with a spatula, to understand if it would hold its structure or de-assemble. This was done after samples were left for two hours in the oven. In both natural HA and synthetic HA samples, the ones with lower concentration were fully polymerized, revealing that lower concentrations of HA allow a better crosslinking reaction between the intervenient parts (BGP, Ch and HA). The same cannot be said about the higher concentration samples; in fact, although they polymerized well to some extent, not all the solution reacted after two hours.

The sample with the best performance was the SYN_HA (0.125% wt/vol) as it passed these tests distinctively in all categories.

As mentioned in the table, injectability was also tested and the results are shown below. Its discussion takes place in chapter **3.3.1**.

Table 3.1 *Results for the pH, homogeneity and polymerization tests*

Note: ✓✓- very good; ✓- good; **X** - bad.

	Samples	pH	Homogeneity	Injectability	Polymerization
Synthetic	Ch-HA (0.125%)	7	✓✓	✓✓	✓✓
	Ch-HA (0.25%)	7	✓	X	✓
Natural	Ch-HA (0.125%)	7	✓	✓	✓✓
	Ch-HA (0.25%)	7	X	X	✓

3.2.4 Stability tests

With the stability test, it was possible to draw a degradation profile of the PBS immersed hydrogels, by measuring their weight on different timepoints. With this weight, the weight loss was calculated and translated in the graph shown below (**Figure 3.4**).

Analyzing the figure underneath, it is possible to see that in both hydrogels there is an initial accentuated loss of weight. This corresponds to the first 24h, where the initial measure is of the dry hydrogel immediately after being removed from the oven, and the following is of the hydrogel already immersed in PBS. In the first day, for both hydrogels, there is an accentuated weight loss. From day 1 to day 10, there is an additional weight loss for both hydrogels, although smaller than for the first 24 hours. This difference was dimmed significant for both cases according to the statistical test performed ($p<0.05$). Comparing the hydrogels between each other, graphs show that they both reached a plateau and are therefore stable after the first 24 h. Nonetheless, from the beginning, it's clear that the hydrogel with 0.25% wt/vol HA (blue), as opposed to the 0.125% wt/vol HA (green) one, had the most weight loss overall. This could be explained by a reduced polymerization phase resulted from the larger amount of HA added, which disturbed the equilibrium between the BGP and chitosan. According to the statistical analysis performed this difference in weight loss between both samples is also significant ($p<0.05$).

It is important that they maintain a stable structure, so that they can provide a durable support for cell proliferation. In both these cases the weight loss revealed to be statistically significant, both between the two hydrogels, as well as individually. However, on the 10th day we see a degradation percentage of 40% for the 0.25% wt/vol one and an even lower one of 30% for the 0.125% one. When compared to the stability of the hydrogel without HA, made

by Stanzione et al [38] given that the Ch-only had a 63% weight loss percentage it is possible to say that the addition of HA made a positive impact in stability. Between the two of them, Ch-HA (0.125% wt/vol) has a better profile since the weight loss was smaller.

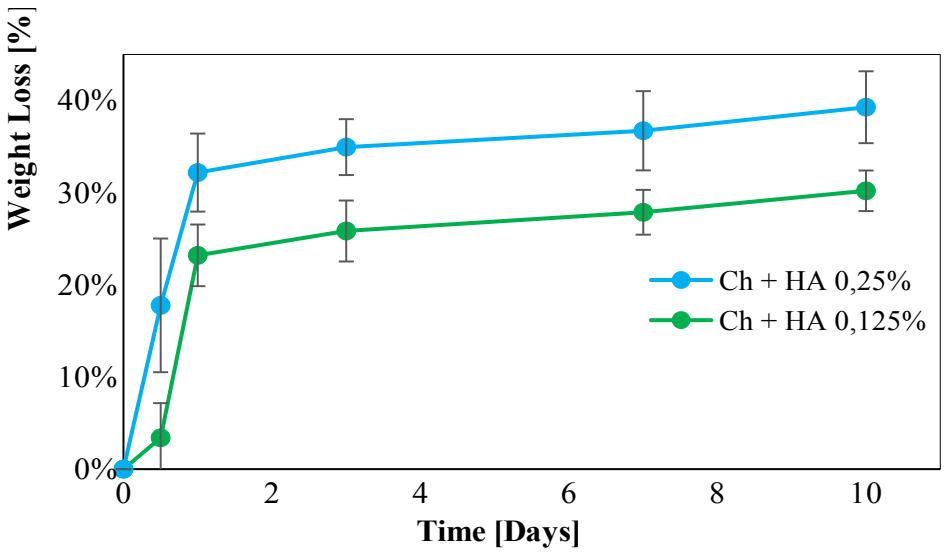

Figure 3.4 *Stability test: weight loss trend of the Ch-HA hydrogels in a time period of 10 days.*

3.2.3 Compression test

The displacement and applied force were normalized over the initial thickness and sample area, correspondingly. Consequently, the normalized parameters were stress (N/mm2 = kPa) and strain (mm/mm). As an example, the stress-strain curve of the three Ch-HA (0.125% wt/vol) hydrogel samples are shown in **Figure 3.5** - A. The stress-strain curve of the three Ch-HA (0.25% wt/vol) hydrogel samples are reported in **APPENDIX 1 - A**.

Hydrogels are polymeric materials, so it is expected that their strain/stress curve describes a non-linear elastic deformation. With the applied force increasing, the internal forces of the hydrogel also increase creating stress. Ultimately this will cause a slower rise in the deformation, as the internal forces of the material tend to contradict the force applied so the hydrogel doesn't collapse. This will increase the non-linearity of the curve. In order to obtain the Young's modulus of a stress/strain curve, linearity is a requirement. As a result, in order to estimate the stiffness of the hydrogels, the Young's modulus was determined for both types of hydrogels in the first linear region of the stress-strain curve, specifically in the 0-5% strain range (**Figure 3.5 - B**) (**APPENDIX 1 - B** for the Ch-HA (0.25% wt/vol) hydrogel samples).

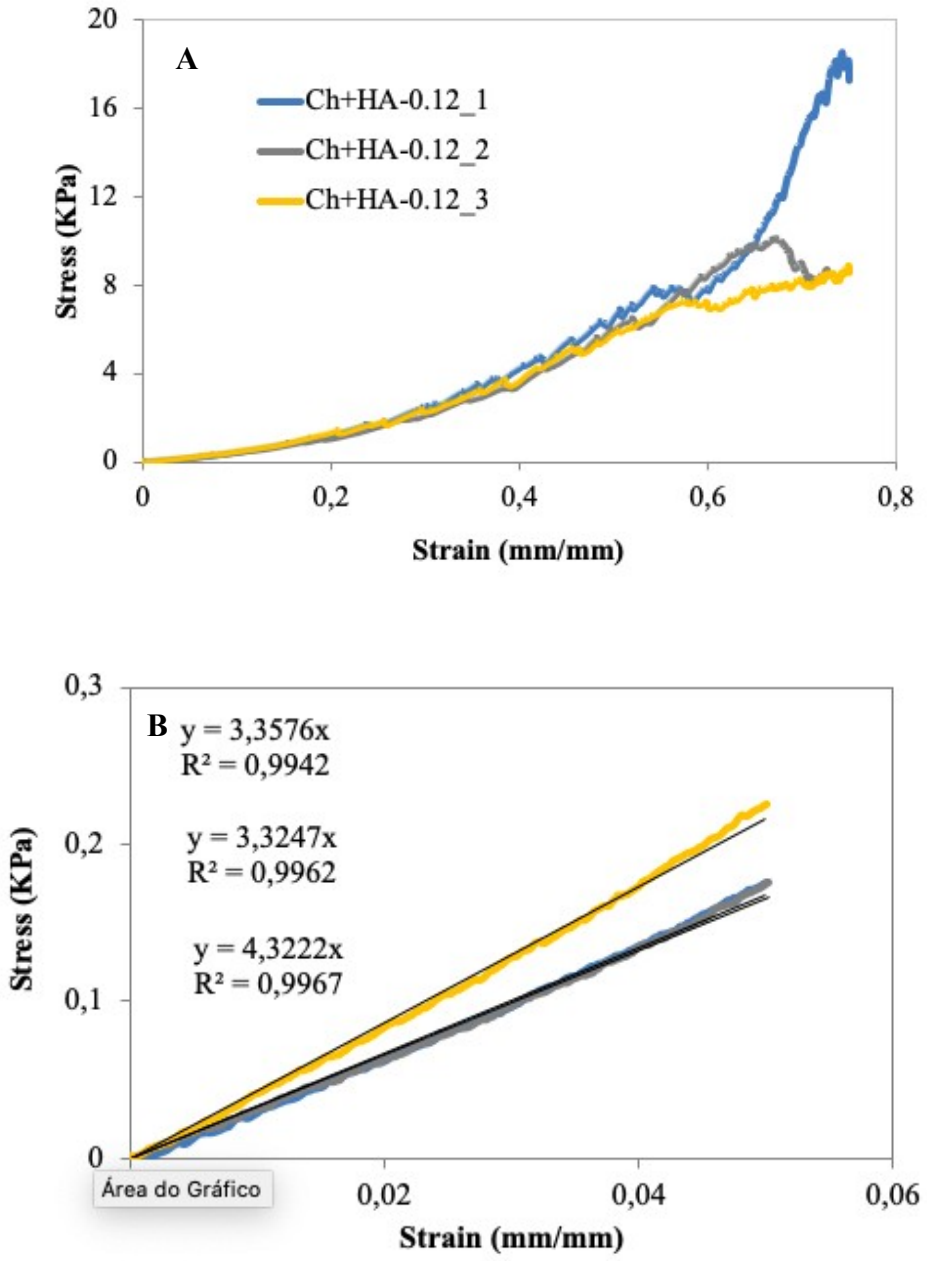

Figure 3.5 *(A) Stress-strain curve of the Ch-HA (0.125%) hydrogels, (B) Linear range of the stress-strain curve used to calculate the Young's modulus, related to the Ch-HA (0,125%) hydrogels.*

The mechanical test results are reported in **Figure 3.6**.

The mean of the Young's modulus calculated at low strain values, 0 – 5%, was about 3.66 kPa for the 0.125% wt/vol HA hydrogels ($\sigma = 0.57$) and about 3.30 kPa for the 0.25% wt/vol HA ones ($\sigma = 0.21$). The Young's modulus of the Ch-HA at 0.125% wt/vol hydrogels was not substantially greater than that of the Ch-HA 0.25% wt/vol ones ($p >> 0.05$). Because the polymerization time for both types of hydrogels was the same (2 hours), and the only

difference between them was the percentage of hydroxyapatite present, these results suggested that, while the hydrogel with the smaller percentage in HA showed a higher modulus of elasticity, the difference was not statistically significant.

Considering that the Young's modulus indicates the stiffness of a material, through the graph we could conclude that the Ch-HA (0.125% wt/vol) hydrogel has a higher polymerization ability than the 0.25% wt/vol one, although as mentioned before, not statistically relevant. These results are in agreement to the stability test performed as 0.125% wt/vol concentration also showed higher stability.

According to the results obtained from this test individually, both hydrogels, when compared to each other, don't present significant differences in stiffness, which means that both appear to be suitable for their intended purpose.

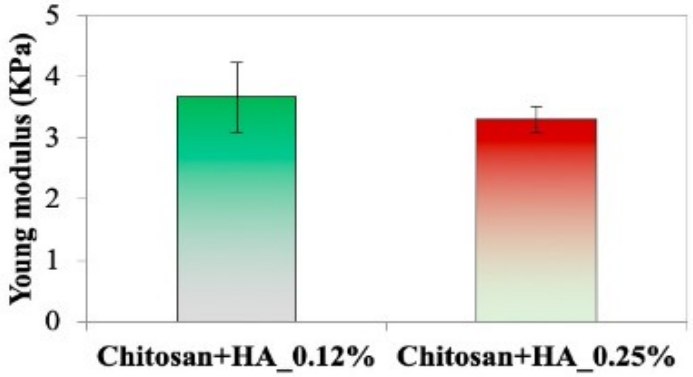

Figure 3.6 *Compression test final results: Comparison of the Young's modulus values of the Ch+HA (0.125% wt/vol) hydrogel and the Ch+HA (0.25% wt/vol) hydrogel.*

3.3. Bioprinting

Although several concentrations of synthetic and natural Hydroxyapatite incorporated in the Chitosan hydrogels were tested, only the ones with 0.125% and 0.25% wt/vol produced satisfactory results. The concentrations above 0.25% wt/vol tested (0.5%, 0.65%, 0.7%, 0.8%, 0.9%, 1% wt/vol) performed poorly in preliminary tests like homogeneity and injectability due clusters of aggregated particles. Either way bioprinting was still tested using a 0.66mm conic needle, to avoid clogging. The use of this needle, however, did not give good results; the 3D structures, in fact, were too large and did not hold a shape, and merged. Additionally, each segment that was dispensed had a much larger diameter than the size of the tip of the needle. This could not be optimized with the bioprinter parameters; therefore, it is likely that

the formulation caused the dispensed material to be unsuitable for bioprinting. The fact that the material did not become more consistent with the addition of HA was surprising, because in many studies the incorporation of this material "*improves stiffness, interconnectivity, and osteogenic potential in collagen-based scaffolds for bone tissue engineering applications*". [47]

3.3.1 Bioink printability

A manual dispensing test was performed on both NAT_HA and SYN_HA to assess the compatibility of the Ch-HA hydrogel (at 0.125% and 0.25% wt/vol) for 3D extrusion-based bioprinting.

This test was done to understand the capability of the samples to be dispensed in a continuous manner and also to understand if the HA particles are able to go through the conic needle without obstruction. The size of the tip used was 0.41 mm. Considering the dimensions of the particles seen from SEM, in theory all samples should go through the needle. However, as already stated above, HA tends to create clusters of nanocrystals. To try to minimize this, the samples were taken to vortex and sonication prior to the testing moment.

As shown in **table 3.1**, the SYN_HA (0.125% wt/vol) sample performed the best. The hydrogel was dispensed and formed a fiber shaped formation and layer stacking, indicating that it is printable and suitable for 3D extrusion-based bioprinting. The fibers were quite uniform and held their shape without breaking or separating as shown in **Figure 3.7**. The other samples seemed to dispense in drop formation and merged completely. Neither of them had any obstruction problems with the needle.

Figure 3.7 *(Left) Fiber formation and (Right) example of structure Bioprinted with 0.125% wt/vol SYN_HA.*

3.3.2 parameters optimization

Considering all the previous results, the SYN_HA hydrogels of 0.125% and 0.25% wt/vol were bioprinted with a 0.41 mm conic needle and the bioprinter parameters optimized. Previous work was already done by Stanzione et al [38]to optimize the chitosan-only-based hydrogels; the study showed the best printing conditions were a pressure of 10 KPa, at a range of temperatures between 20-25ºC and at a robot speed of 2 mm/s. These parameters were considered as a starting point to optimize the printing of the composite hydrogels.

For the 0.125% wt/vol hydrogel, several pressures were tested: 12kPa, 15kPa, 18kPa and 20kPa. Only the 18kPa and 20kPa pressures were able to print the 3 lines successfully (**Figure 3.8**). As for the 0.25% wt/vol, the same pressures were tested with an additional one of 30kPa. Only 20kPa and 30kPa were able to print 3 lines successfully. Some robot speeds were tested 2-10 mm/s but only the 2mm/s speed was able to give good results. This could be attributed to the fact that the samples are thermosensitive and, in this case, the bioprinter did not possess a cooling system, making the samples very susceptible to the room temperature.

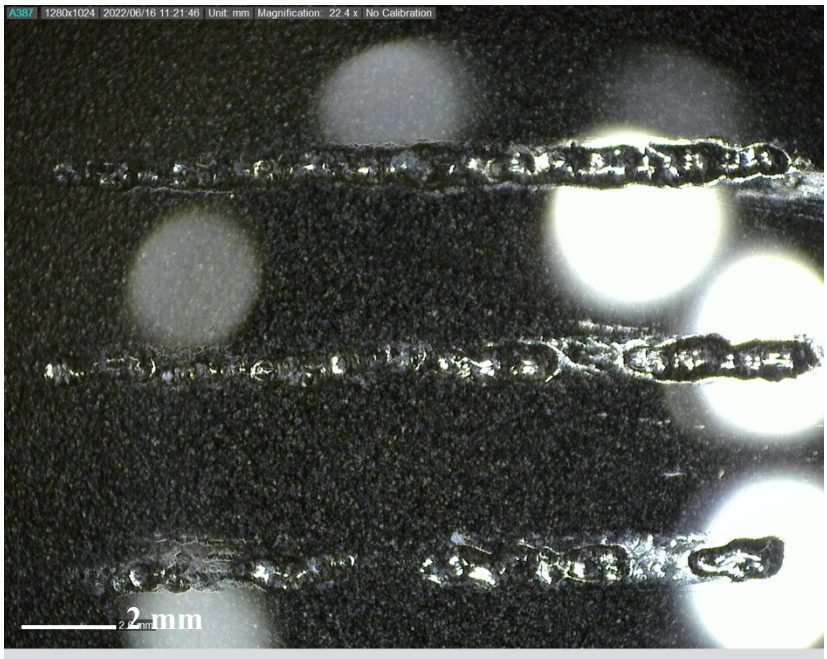

Figure 3.8 *Picture captured by Dinolight of 3 bioprinted lines, ready to be measured.*

By comparing the strand thickness with the needle diameter (0.41mm), the pressure that allowed us to more precisely reproduce the printing conditions was that one of 18 kPa with the 0.125% wt/vol concentration (see **Figure 3.9** for all the results). This sample at this pressure, resulted in the closest strand thickness to the needle diameter.

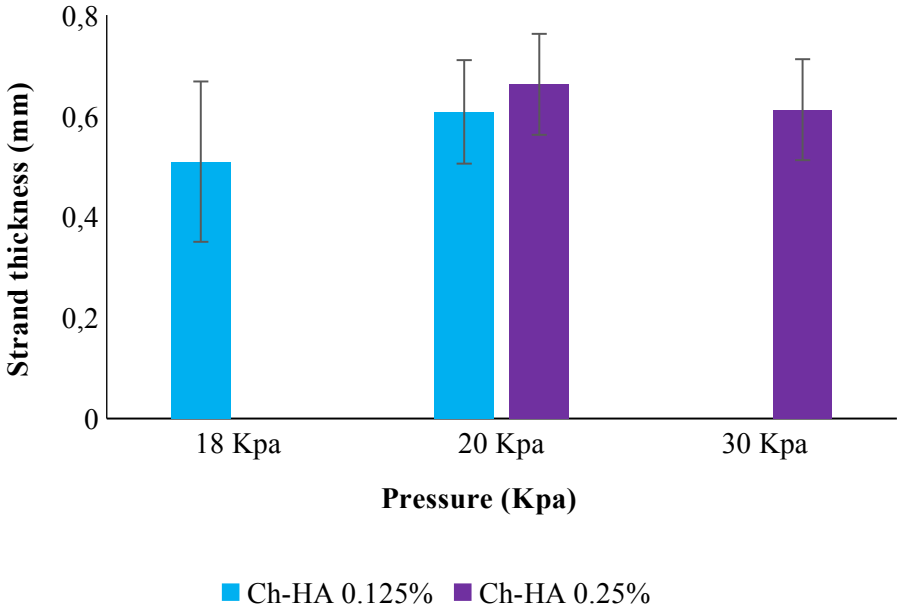

Figure 3.9 *Graph showing the different diameters of extruded strand when a different pressure is applied in both 0.125% wt/vol and 0.25% wt/vol*

4. CONCLUSION

In this work the synthesis, characterization, and 3D extrusion-based bioprinting of a chitosan-hydroxyapatite based (Ch-HA) bioinks for bone regeneration was carried out. The synthesis of HA nanocrystals, followed by the protocol used by Iafisco et al [50] and the chitosan-based hydrogel described by Stanzione et al [38], allowed the creation of a temperature sensitive hydrogel with increased abilities when compared with the chitosan-only based hydrogel. When exposed to a temperature of 37ºC for two consecutive hours, it fully polymerizes.

Several concentrations of the SYN_HA incorporated were tested, being that the final comparison stood between 0.25 wt/vol% of HA or 0.125 wt/vol%. The proportion between chitosan and the betaglycerophosphate (BGP) remained the same as the protocol mentioned, with a ratio of 3:2, respectively.

Then, HA nanocrystals and after the Ch-HA hydrogel were subjected to several tests in order to characterize them and gather information. The results were the following:

- Both natural and synthetic HA nanoparticles showed high purity, with no additional compound present.

- SEM analysis showed that natural HA nanocrystals size range from 200nm to 600nm and that SYN_HA nanocrystals size range from 19nm to 180nm, making them the most suited for biomedical in vivo application.

- The stability test for SYN_HA showed that in both concentration there was a statistically significant decrease in weight in such a short time period. About 40% for 0.25% wt/vol one and 30% for the 0.125% wt/vol one. When compared to the stability of the hydrogel with only Ch, whose weight loss was about 63% in the same time period, then it was proved that the addition of HA made a positive impact in stability. The hydrogel with the lowest HA concentration however (0.125% wt/vol) was the one chosen as the “best” since it has the lowest degradation.

- The Youngs modulus obtained after the compression test indicated that when it came to stiffness, the difference in value between the hydrogels was nor significant. The value for the 0.125 wt/vol% one was 3.66 KPa and the value for the 0.25 wt/vol% one was 3.30 KPa.

All these tests allowed us to confirm the use of Ch-HA-based hydrogel with a synthetic HA concentration of 0.125 wt/vol% as a biomaterial ink for 3D extrusion-based bioprinting, since it possessed most of the necessary characteristics (appropriate particle size and purity of

the nanocrystals, pH, best homogeneity and polymerization, and appropriated stiffness) that make it suitable for future support on cell encapsulation.

The optimization of bioprinting parameters was executed in order to comprehend which was the best printing pressure for Ch-HA hydrogel; the results attained implied that extrusion pressure of 18 KPa trough a tapered needle, 20°C of temperature and a robot speed of 4mm/s were the best parameters.

To sum up, the Ch-HA-based (synthetic - 0.125 wt/ vol%) hydrogel developed had the most suitable characteristics to be used as biomaterial ink for 3D extrusion-based bioprinting.

The future development of this work will be to test the hydrogel identified in this thesis work for the realization of a 3D scaffold with suitable characteristics of osteogenic differentiation for application in bone tissue engineering.

5. FUTURE WORK

There are still some properties to still be tested to obtain a bioink with the most satisfactory properties. In the future it would be imperative to do a swelling test on the hydrogels as it is an important characteristic to assess.

After the hydrogel characteristics and stability are fully optimized, the next step would be the incorporation of cells in the biomaterial ink, making it a bioink. The key points to address are the type of cells to use, and possible changes in the bioprinter parameters with cell incorporation in the hydrogels.

Finally, it would also be interesting, from a sustainable point of view, to make the NAT_HA nanocrystals fitting for the hydrogel incorporation. The size range would have to be reduced, and the optimization of the bioprinting characteristics might have to be fine-tuned; with the appropriate parameters, the performance of the bioink should be exactly the same of those based on SYN_HA, making this an important substitute in the future in the area of bone regeneration.

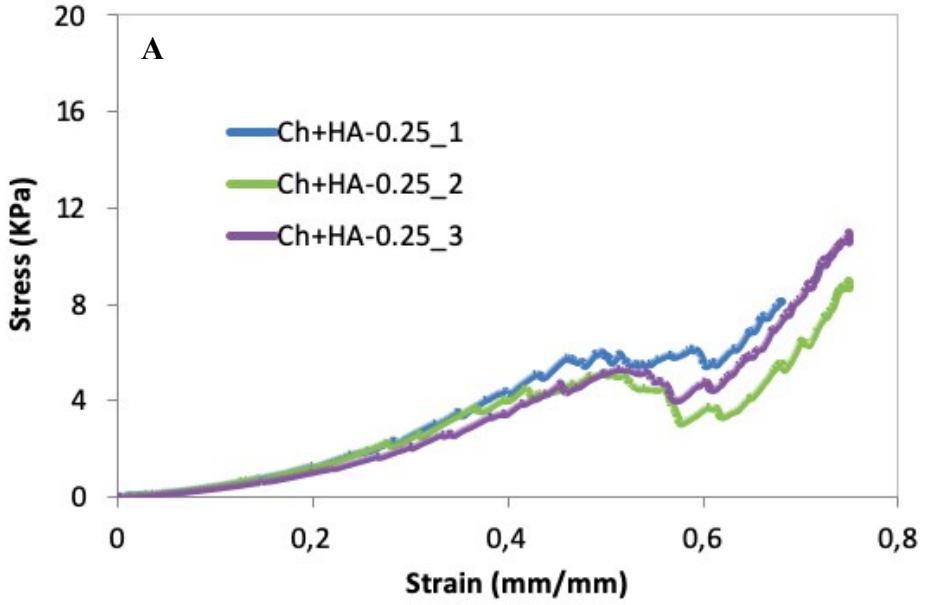
A
Ch+HA-0.25_1
Ch+HA-0.25_2
Ch+HA-0.25_3
Stress (KPa)
Strain (mm/mm)
0
4
8
12
16
20
0
0,2
0,4
0,6
0,8

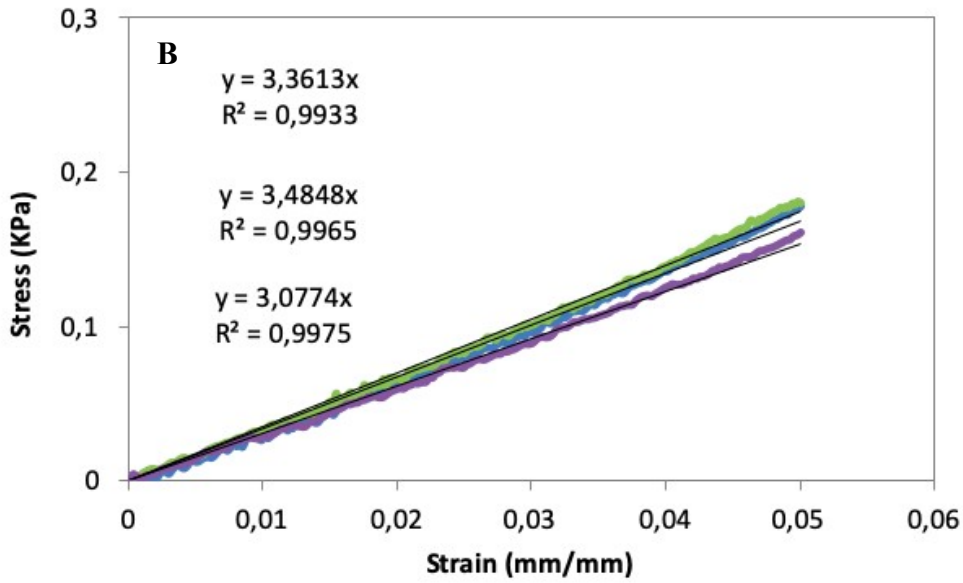
B
y = 3,3613x
R² = 0,9933
y = 3,4848x
R² = 0,9965
y = 3,0774x
R² = 0,9975
Stress (KPa)
Strain (mm/mm)
0
0,1
0,2
0,3
0
0,01
0,02
0,03
0,04
0,05
0,06

REFERENCES

[1] L. Liedert, Astrid Kaspar, Daniela Augat, Peter Ignatius, Anita Claes, 'Mechanobiology of Bone Tissue and Bone Cells', in *Mechanosensitivity in Cells and Tissues.*, I. Kamkin, A Kiseleva, Ed. 2005.

[2] R. A. D. Carano and E. H. Filvaroff, 'Angiogenesis and bone repair', *Drug Discov. Today*, vol. 8, no. 21, pp. 980–989, 2003, doi: 10.1016/S1359-6446(03)02866-6.

[3] P. Jukka *et al.*, 'Mesenchymal Stem Cell-macrophage Crosstalk and Bone Healing', *Biomaterials*, vol. 196, pp. 80–89, 2019, doi: 10.1016/j.biomaterials.2017.12.025.Mesenchymal.

[4] R. Cancedda, P. Giannoni, and M. Mastrogiacomo, 'A tissue engineering approach to bone repair in large animal models and in clinical practice', *Biomaterials*, vol. 28, no. 29, pp. 4240–4250, 2007, doi: 10.1016/j.biomaterials.2007.06.023.

[5] T. Genova, I. Roato, M. Carossa, C. Motta, D. Cavagnetto, and F. Mussano, 'Advances on bone substitutes through 3d bioprinting', *Int. J. Mol. Sci.*, vol. 21, no. 19, pp. 1–28, 2020, doi: 10.3390/ijms21197012.

[6] Q. L. Loh and C. Choong, 'Three-dimensional scaffolds for tissue engineering applications: Role of porosity and pore size', *Tissue Eng. - Part B Rev.*, vol. 19, no. 6, pp. 485–502, 2013, doi: 10.1089/ten.teb.2012.0437.

[7] R. Edmondson, J. J. Broglie, A. F. Adcock, and L. Yang, 'Three-dimensional cell culture systems and their applications in drug discovery and cell-based biosensors', *Assay Drug Dev. Technol.*, vol. 12, no. 4, pp. 207–218, 2014, doi: 10.1089/adt.2014.573.

[8] R. Hudák, M. Trebuňová, J. Živčák, and D. Kottfer, 'Scaffolds for Tissue Engineering – Introduction', *Acta Tecnol.*, vol. 4, no. 4, pp. 67–70, 2018, doi: 10.22306/atec.v4i4.43.

[9] C. M. Murphy, F. J. O'Brien, D. G. Little, and A. Schindeler, 'Cell-scaffold interactions in the bone tissue engineering triad', *Eur. Cells Mater.*, vol. 26, pp. 120–132, 2013, doi: 10.22203/eCM.v026a09.

[10] R. Mhanna and A. Hasan, '1 Introduction to Tissue Engineering', in *Tissue Engineering for Artificial Organs: Regenerative Medicine, Smart Diagnostics and Personalized Medicine*, 2017, pp. 3–34.

[11] A. J. Engler, S. Sen, H. L. Sweeney, and D. E. Discher, 'Matrix Elasticity Directs Stem

Cell Lineage Specification', *Cell*, vol. 126, no. 4, pp. 677–689, 2006, doi: 10.1016/j.cell.2006.06.044.

[12] M. P. Nikolova and M. S. Chavali, 'Recent advances in biomaterials for 3D scaffolds: A review', *Bioact. Mater.*, vol. 4, no. October, pp. 271–292, 2019, doi: 10.1016/j.bioactmat.2019.10.005.

[13] E. Saiz, E. A. Zimmermann, J. S. Lee, U. G. K. Wegst, and A. P. Tomsia, 'Perspectives on the role of nanotechnology in bone tissue engineering', *Dent. Mater.*, vol. 29, no. 1, pp. 103–115, 2013, doi: 10.1016/j.dental.2012.08.001.

[14] J. An, J. E. M. Teoh, R. Suntornnond, and C. K. Chua, 'Design and 3D Printing of Scaffolds and Tissues', *Engineering*, vol. 1, no. 2, pp. 261–268, 2015, doi: 10.15302/J-ENG-2015061.

[15] M. Whitaker, 'The history of 3D printing in healthcare. The Bulletin of the Royal College of Surgeons of England. 2014;96(7):228-229.', *Bull. R. Coll. Surg. Engl.*, vol. 96, no. 7, pp. 17–19, 2015.

[16] E. J. Hurst, '3D Printing in Healthcare: Emerging Applications', *J. Hosp. Librariansh.*, vol. 16, no. 3, pp. 255–267, 2016, doi: 10.1080/15323269.2016.1188042.

[17] C. Mandrycky, Z. Wang, K. Kim, and D. H. Kim, '3D bioprinting for engineering complex tissues', *Biotechnol. Adv.*, vol. 34, no. 4, pp. 422–434, 2016, doi: 10.1016/j.biotechadv.2015.12.011.

[18] S. Derakhshanfar, R. Mbeleck, K. Xu, X. Zhang, W. Zhong, and M. Xing, '3D bioprinting for biomedical devices and tissue engineering: A review of recent trends and advances', *Bioact. Mater.*, vol. 3, no. 2, pp. 144–156, 2018, doi: 10.1016/j.bioactmat.2017.11.008.

[19] S. V. Murphy and A. Atala, '3D bioprinting of tissues and organs', *Nat. Biotechnol.*, vol. 32, no. 8, pp. 773–785, 2014, doi: 10.1038/nbt.2958.

[20] Z. Xie, M. Gao, A. O. Lobo, and T. J. Webster, '3D bioprinting in tissue engineering for medical applications: The classic and the hybrid', *Polymers (Basel).*, vol. 12, no. 8, 2020, doi: 10.3390/POLYM12081717.

[21] J. Malda *et al.*, '25th anniversary article: Engineering hydrogels for biofabrication', *Adv. Mater.*, vol. 25, no. 36, pp. 5011–5028, 2013, doi: 10.1002/adma.201302042.

[22] F. You, B. F. Eames, and X. Chen, 'Application of extrusion-based hydrogel bioprinting for cartilage tissue engineering', *Int. J. Mol. Sci.*, vol. 18, no. 7, pp. 8–14, 2017, doi: 10.3390/ijms18071597.

[23] I. T. Ozbolat and M. Hospodiuk, ‘Current advances and future perspectives in extrusion-based bioprinting’, *Biomaterials*, vol. 76, pp. 321–343, 2016, doi: 10.1016/j.biomaterials.2015.10.076.

[24] J. Groll *et al.*, ‘A definition of bioinks and their distinction from biomaterial inks’, *Biofabrication*, vol. 11, no. 1, 2019, doi: 10.1088/1758-5090/aaec52.

[25] S. Kyle, Z. M. Jessop, A. Al-Sabah, and I. S. Whitaker, ‘“Printability’’ of Candidate Biomaterials for Extrusion Based 3D Printing: State-of-the-Art”’, *Adv. Healthc. Mater.*, vol. 6, no. 16, pp. 1–16, 2017, doi: 10.1002/adhm.201700264.

[26] D. F. Williams, ‘On the mechanisms of biocompatibility’, *Biomaterials*, vol. 29, no. 20, pp. 2941–2953, 2008, doi: 10.1016/j.biomaterials.2008.04.023.

[27] W. Wang, R. Narain, and H. Zeng, *Hydrogels*. Elsevier Inc., 2020.

[28] J. M. Unagolla and A. C. Jayasuriya, ‘Hydrogel-based 3D bioprinting: A comprehensive review on cell-laden hydrogels, bioink formulations, and future perspectives’, *Appl. Mater. Today*, vol. 18, no. xxxx, p. 100479, 2020, doi: 10.1016/j.apmt.2019.100479.

[29] H. Cui, M. Nowicki, J. P. Fisher, and L. G. Zhang, ‘3D Bioprinting for Organ Regeneration’, *Adv. Healthc. Mater.*, vol. 6, no. 1, 2017, doi: 10.1002/adhm.201601118.

[30] H. J. Chung and T. G. Park, ‘Self-assembled and nanostructured hydrogels for drug delivery and tissue engineering’, *Nano Today*, vol. 4, no. 5, pp. 429–437, 2009, doi: 10.1016/j.nantod.2009.08.008.

[31] J. Zhu, ‘Stress Risk Assessment Form’, *Expert Rev.Med.Devices*, vol. 8, no. 5, pp. 607–626, 2011.

[32] M. C. Gomez-Guillen, B. Gimenez, M. E. Lopez-Caballero, and M. P. Montero, ‘Functional and bioactive properties of collagen and gelatin from alternative sources: A review’, *Food Hydrocoll.*, vol. 25, no. 8, pp. 1813–1827, 2011, doi: 10.1016/j.foodhyd.2011.02.007.

[33] M. M. Khansari *et al.*, ‘Classification of Hydrogels Based on Their Source: A Review and Application in Stem Cell Regulation’, *Jom*, vol. 69, no. 8, pp. 1340–1347, 2017, doi: 10.1007/s11837-017-2412-9.

[34] A. Ali and S. Ahmed, ‘Recent Advances in Edible Polymer Based Hydrogels as a Sustainable Alternative to Conventional Polymers’, *J. Agric. Food Chem.*, vol. 66, no. 27, pp. 6940–6967, 2018, doi: 10.1021/acs.jafc.8b01052.

[35] K. W. Jiang, Weiqian Li, Mingqiang Chen, Zaozao Leong, ‘Cell-laden Microfluidic Microgels for Tissue Regeneration’, *Lab Chip*, vol. 16, no. 23, pp. 4482–4506, 2016, doi: 10.1039/c6lc01193d.

[36] M. Ermis *et al.*, *Hydrogels as a new platform to recapitulate the tumor microenvironment*. Elsevier Inc., 2018.

[37] R. Parhi, ‘Cross-linked hydrogel for pharmaceutical applications: A review’, *Adv. Pharm. Bull.*, vol. 7, no. 4, pp. 515–530, 2017, doi: 10.15171/apb.2017.064.

[38] A. Stanzione *et al.*, ‘Thermosensitive chitosan-based hydrogels supporting motor neuron-like NSC-34 cell differentiation’, *Biomater. Sci.*, vol. 9, no. 22, pp. 7492–7503, 2021, doi: 10.1039/d1bm01129d.

[39] M. Sun, X. Sun, Z. Wang, S. Guo, G. Yu, and H. Yang, ‘Synthesis and properties of gelatin methacryloyl (GelMA) hydrogels and their recent applications in load-bearing tissue’, *Polymers (Basel).*, vol. 10, no. 11, 2018, doi: 10.3390/POLYM10111290.

[40] S. Young, M. Wong, Y. Tabata, and A. G. Mikos, ‘Gelatin as a delivery vehicle for the controlled release of bioactive molecules’, *J. Control. Release*, vol. 109, no. 1–3, pp. 256–274, 2005, doi: 10.1016/j.jconrel.2005.09.023.

[41] Z. Dong, Q. Yuan, K. Huang, W. Xu, G. Liu, and Z. Gu, ‘Gelatin methacryloyl (GelMA)-based biomaterials for bone regeneration’, *RSC Adv.*, vol. 9, no. 31, pp. 17737–17744, 2019, doi: 10.1039/c9ra02695a.

[42] R. Jayakumar, M. Prabaharan, S. V. Nair, S. Tokura, H. Tamura, and N. Selvamurugan, ‘Novel carboxymethyl derivatives of chitin and chitosan materials and their biomedical applications’, *Prog. Mater. Sci.*, vol. 55, no. 7, pp. 675–709, 2010, doi: 10.1016/j.pmatsci.2010.03.001.

[43] J. O. Gonçalves *et al.*, ‘Chitosan-Based Hydrogels’, in *Sustainable agriculture reviews*, 2019, pp. 147–173.

[44] C. Piccirillo *et al.*, ‘Extraction and characterisation of apatite- and tricalcium phosphate-based materials from cod fish bones’, *Mater. Sci. Eng. C*, vol. 33, no. 1, pp. 103–110, 2013, doi: 10.1016/j.msec.2012.08.014.

[45] M. Habibah, Tutut Ummul Amlani, Dharanshi V. Brizuela, *Hydroxyapatite Dental Material*. 2022.

[46] R. N. Granito, A. C. M. Renno, H. Yamamura, M. C. de Almeida, P. L. M. Ruiz, and D. A. Ribeiro, ‘Hydroxyapatite from fish for bone tissue engineering: A promising approach’, *Int. J. Mol. Cell. Med.*, vol. 7, no. 2, pp. 80–90, 2018, doi:

10.22088/IJMCM.BUMS.7.2.80.

[47] S. Dhivya, S. Saravanan, T. P. Sastry, and N. Selvamurugan, 'Nanohydroxyapatite-reinforced chitosan composite hydrogel for bone tissue repair in vitro and in vivo', *J. Nanobiotechnology*, vol. 13, no. 1, pp. 1–13, 2015, doi: 10.1186/s12951-015-0099-z.

[48] B. Cengiz, Y. Gokce, N. Yildiz, Z. Aktas, and A. Calimli, 'Synthesis and characterization of hydroxyapatite nanoparticles', *Colloids Surfaces A Physicochem. Eng. Asp.*, vol. 322, no. 1–3, pp. 29–33, 2008, doi: 10.1016/j.colsurfa.2008.02.011.

[49] Z. Bal, T. Kaito, F. Korkusuz, and H. Yoshikawa, 'Bone regeneration with hydroxyapatite-based biomaterials', *Emergent Mater.*, vol. 3, no. 4, pp. 521–544, 2020, doi: 10.1007/s42247-019-00063-3.

[50] M. Iafisco *et al.*, 'Nanocrystalline carbonate-apatites: Role of Ca/P ratio on the upload and release of anticancer platinum bisphosphonates', *Nanoscale*, vol. 4, no. 1, pp. 206–217, 2012, doi: 10.1039/c1nr11147g.

[51] A. I. Van Den Bulcke, B. Bogdanov, N. De Rooze, E. H. Schacht, M. Cornelissen, and H. Berghmans, 'Structural and Rheological Properties of Methacrylamide Modified Gelatin Hydrogels', *Biomacromolecules*, vol. 1, no. 1, pp. 31–38, 2000.

[52] T. R. Shah, H. Koten, and H. M. Ali, *Performance effecting parameters of hybrid nanofluids*. INC, 2020.

[53] M. H. Boratto, 'Semiconducting and Insulating oxides applied to electronic devices', Universidade Estadual Paulista "Júlio de Mesquita Filho" - UNESP, 2018.

[54] M. Omidi *et al.*, *Characterization of biomaterials*. Elsevier Ltd, 2017.

[55] Y. Wang and V. Petrova, 'Scanning electron microscopy', in *Nanotechnology Research Methods for Foods and Bioproducts*, 1st ed., 2012, p. 103.126.

[56] R. Arunachalam and P. K. Krishnan, *Compressive Response of Aluminum Metal Matrix Composites*. Elsevier Ltd., 2021.

[57] N. Paxton, W. Smolan, T. Böck, F. Melchels, J. Groll, and T. Jungst, 'Proposal to assess printability of bioinks for extrusion-based bioprinting and evaluation of rheological properties governing bioprintability', *Biofabrication*, vol. 9, no. 4, 2017, doi: 10.1088/1758-5090/aa8dd8.

[58] B. Y. S. Kumar, A. M. Isloor, G. C. M. Kumar, Inamuddin, and A. M. Asiri, 'Nanohydroxyapatite Reinforced Chitosan Composite Hydrogel with Tunable Mechanical and Biological Properties for Cartilage Regeneration', *Sci. Rep.*, vol. 9, no. 1, pp. 1–13, 2019, doi: 10.1038/s41598-019-52042-7.

[59] F. Lebre, R. Sridharan, M. J. Sawkins, D. J. Kelly, F. J. O'Brien, and E. C. Lavelle, 'The shape and size of hydroxyapatite particles dictate inflammatory responses following implantation', *Sci. Rep.*, vol. 7, no. 1, pp. 1–13, 2017, doi: 10.1038/s41598-017-03086-0.

[60] P. Sutthavas, P. Habibovic, and S. H. Van Rijt, 'The shape-effect of calcium phosphate nanoparticle based films on their osteogenic properties', *Biomater. Sci.*, vol. 9, no. 5, pp. 1754–1766, 2021, doi: 10.1039/d0bm01494j.

[61] Y. Cai *et al.*, 'Role of hydroxyapatite nanoparticle size in bone cell proliferation', *J. Mater. Chem.*, vol. 17, no. 36, pp. 3780–3787, 2007, doi: 10.1039/b705129h.